A&A 445, 939–958 (2006)
DOI: 10.1051/0004-6361:20053796

Astronomy & Astrophysics

uvby-β photometry of high-velocity and metal-poor stars

XI. Ages of halo and old disk stars⋆,⋆⋆

W. J. Schuster[1], A. Moitinho[2], A. Márquez[3], L. Parrao[4], and E. Covarrubias[5]

[1] Observatorio Astronómico Nacional, UNAM, Apartado Postal 877, Ensenada, BC, CP 22800, Mexico
e-mail: schuster@astrosen.unam.mx
[2] CAAUL, Observatório Astronómico de Lisboa, Tapada da Ajuda, 1349-018 Lisbon, Portugal
e-mail: andre@oal.ul.pt
[3] Instituto Nacional de Astrofísica, Óptica y Electrónica, Luis Enrique Erro No. 1, Tonantzintla, Puebla, CP 72840, Mexico
e-mail: amarquez@inaoep.mx
[4] Institute of Astronomy, UNAM, México, DF, CP 04510, Mexico
e-mail: laura@astroscu.unam.mx
[5] Universidad de las Americas, San Pedro Cholula, Puebla, CP 72820, Mexico

Received 8 July 2005 / Accepted 13 September 2005

ABSTRACT

New *uvby–β* data are provided for 442 high-velocity and metal-poor stars; 90 of these stars have been observed previously by us, and 352 are new. When combined with our previous two photometric catalogues, the data base is now made up of 1533 high-velocity and metal-poor stars, all with *uvby–β* photometry and complete kinematic data, such as proper motions and radial velocities taken from the literature. Hipparcos, plus a new photometric calibration for M_v also based on the Hipparcos parallaxes, provide distances for nearly all of these stars; our previous photometric calibrations give values for $E(b-y)$ and [Fe/H]. The [Fe/H], V(rot) diagram allows us to separate these stars into different Galactic stellar population groups, such as old-thin-disk, thick-disk, and halo. The X histogram, where X is our stellar-population discriminator combining V(rot) and [Fe/H], and contour plots for the [Fe/H], V(rot) diagram both indicate two probable components to the thick disk. These population groups and Galactic components are studied in the $(b-y)_0$, M_v diagram, compared to the isochrones of Bergbusch & VandenBerg (2001, ApJ, 556, 322), to derive stellar ages. The two thick-disk groups have the mean characteristics: ([Fe/H], V(rot), Age, $\sigma_{W'}$) ≈ (−0.7 dex, 120 km s^{-1}, 12.5 Gyr, 62.0 km s^{-1}), and ≈(−0.4, 160, 10.0, 45.8). The seven most metal-poor halo groups, $-2.31 \leq$ [Fe/H] ≤ -1.31, show a mean age of 13.0 ± 0.2 (mean error) Gyr, giving a mean difference from the WMAP results for the age of the Universe of 0.7 ± 0.3 Gyr. These results for the ages and components of the thick disk and for the age of the Galactic halo field stars are discussed in terms of various models and ideas for the formation of galaxies and their stellar populations.

Key words. stars: fundamental parameters – Galaxy: evolution – Galaxy: formation – Galaxy: halo – Galaxy: kinematics and dynamics – Hertzsprung-Russell (HR) and C-M diagrams

1. Introduction

In this day and age of Hubble deep fields, large-scale surveys (for example, Newberg et al. 2002; Schneider et al. 2003; Yanny et al. 2003), WMAP (Bennett et al. 2003), and ΛCDM models of hierarchical galaxy formation, astronomers and cosmologists are moving closer to an understanding of the fundamentals of galaxy formation and early evolution. Within our Galaxy, the detection of the accreting dwarf galaxies in Sagittarius (Ibata et al. 1994) and Canis Major (Martin et al. 2004; Bellazzini et al. 2004) have provided observational evidence and details for accretion and merger processes. Tidal debris in the Galaxy has been detected and studied (Ibata et al. 2001, 2003; Newberg et al. 2002; Crane et al. 2003; Yanny et al. 2003; Rocha-Pinto et al. 2003; 2004; Majewski et al. 2004), as well as structure within the thick disk (Gilmore et al. 2002; Parker et al. 2003, 2004) and evidence of counterrotating kinematics of thick disks in external galaxies (Yoachim & Dalcanton 2005). Models tying thick-disk and halo characteristics to hierarchical clustering have been developed (Abadi et al. 2003; Brook et al. 2004). What is shown in this paper is that the data bases developed over the last couple decades

⋆ Based on observations collected at the H.L. Johnson 1.5 m telescope at the Observatorio Astronómico Nacional at San Pedro Mártir, Baja California, Mexico.

⋆⋆ Tables 1 to 4 are only available in electronic form at the CDS via anonymous ftp to cdsarc.u-strasbg.fr (130.79.128.5) or via http://cdsweb.u-strasbg.fr/cgi-bin/qcat?J/A+A/445/939

for the local high-velocity and metal-poor stars (Schuster & Nissen 1988; Schuster et al. 1993; Carney et al. 1994; Ryan 1989) have not yet been totally exploited and exhausted for results concerning the above themes: the age and origins of the Galaxy and its halo; the age, structure, and formation of the Galactic thick disk. In this paper the *uvby–β* photometry for more than 1500 high-velocity and metal-poor stars is applied to these problems of ages, structure, and origins relating to our Galaxy and its stellar populations.

The *uvby–β* photometric system is particularly suited for the study of high-velocity and metal-poor (hereafter, HV) F- and G-type stars, as has already been pointed out in several papers of this series, such as Schuster & Nissen (1988, SN; 1989a, Paper II; 1989b, Paper III), Nissen & Schuster (1991, Paper V), Schuster et al. (1993, SPC), and Márquez & Schuster (1994, MS). Briefly, intrinsic-color calibrations, $(b-y)_0$–β, exist that allow accurate and precise, $\pm 0\overset{\mathrm{m}}{.}01$, measures of interstellar reddening excesses, $E(b-y)$, for individual field stars; such a calibration has been given in Paper II. In this same paper photometric calibrations are given for the [Fe/H] values of F- and G-type stars. Photometric absolute magnitudes and distances can be calibrated and used effectively, as shown in Olsen (1984) and Paper V. This photometric system has the great advantage that it permits us to obtain accurate stellar distances even for evolving main-sequence and subgiant stars due to the gravity sensitivity of the c_0 index. Also, importantly, theoretical isochrones in the $T_{\rm eff}$, $M_{\rm bol}$ diagram can be transformed to the $(b-y)_0$, M_V or $(b-y)_0$, c_0 diagrams for the estimation of relative and/or absolute ages of evolving field stars that are near their respective turn-offs, and in several of the previous papers of this series the isochrones of VandenBerg and co-workers have been used for such purposes, to study the Galactic halo population and to make comparative analyses between the relative ages of the halo and thick-disk stellar populations. Most recently the isochrones of Bergbusch & VandenBerg (2001) have been transformed to the *uvby* photometric system using the color—$T_{\rm eff}$ relations of Clem et al. (2004).

uvby–β photometry also can provide basic stellar atmospheric parameters as a prelude to detailed chemical abundance studies making use of high-resolution spectroscopy and model atmospheres. Several empirical calibrations already exist in the literature for the conversion of $(b-y)_0$ or Hβ to $T_{\rm eff}$ (for example, Alonso et al. 1996; 1999; Ramírez & Meléndez 2005a,b); these calibrations include appropriate metallicity dependences. Index diagrams, such as $(b-y)_0$, c_0, or the reddening-free $[m_1]$, $[c_1]$, or β, $[c_1]$, allow the classification of field stars according to their evolutionary status, permitting us to estimate the stellar surface gravities. This information can also be used as input into the model-atmosphere analyses.

In this paper, *uvby–β* photometry is presented for 442 HV stars, 90 repeated from the previous SN and SPC catalogues and 352 observed for the first time by us; in Sect. 2 the selection criteria of these stars, the observing and reduction techniques for the *uvby–β* data, comparisons of this data with our previous photometric catalogues, and a description of this newest catalogue (Table 1) are given. In Sect. 3 are detailed our corrections for interstellar reddening, our photometric abundances ([Fe/H]), the absolute magnitudes and distances, and our photometric classifications (Table 2) for our total data set. Section 4 describes the kinematic data and Galactic velocities, and Sect. 5, the cleaning of our total sample of binary and variable stars. Section 6 concentrates on the [Fe/H], V(rot) diagram: its appearance and use to separate stellar populations and groups, the stellar-population parameter, X, and its histogram, and contour plots and probable structure in the thick disk. In Sect. 7, several $(b-y)_0$, M_V diagrams with isochrones are given for various thick-disk and halo groupings, plus the [Fe/H], $(b-y)_0$ diagram for all the halo stars of this data base together with the turn-off, main-sequence, and subgiant stars of our very-metal-poor sample; the bluer metal-poor stars and relative stellar ages are discussed. Section 8 provides a comparison of our ages in the form of an age versus [Fe/H] diagram, as well as analyses of these ages, the thick-disk structure, and the bluer metal-poor stars in terms of the WMAP results, thick-disk formation scenarios, and hierarchical clustering and merging theories for galaxy formation in a ΛCDM universe. Finally, Sect. 9 sums it all together, giving our main conclusions.

2. Photometric observations of the high-velocity and metal-poor stars

2.1. Selection of the stars

The stars in the catalogue of this publication, Table 1, have been drawn from several sources. B. W. Carney sent a list of the bluer stars from their survey (Carney et al. 1994) which lacked *uvby–β* photometry, for the purpose of determining stellar photometric ages. S.G. Ryan sent a list of numerous stars lacking *uvby–β* included in various of their spectroscopic studies. The student F. Valera helped draw up a list of stars with [Fe/H] ≤ -2.00 from the literature, including the SN and SPC catalogues, the Carney et al. (1994) survey mentioned above, the lists of Sandage & Fouts (1987), as well as those of Norris & Ryan (1989), the idea being to obtain five or more independent *uvby–β* observations for each of these more metal-poor stars to provide more precise stellar atmospheric parameters for various spectroscopic projects. Stars lacking *uvby–β* photometry were also selected from the lists of Thorburn (1994).

2.2. Observation and reduction techniques

The *uvby–β* data presented here in Table 1 for the HV stars were taken using the H.L. Johnson 1.5 m telescope at the San Pedro Mártir Observatory, Baja California, México (hereafter SPM), and the same six-channel *uvby–β* photoelectric photometer as for the northern observations of SN, all the *uvby–β* observations of SPC, the northern data of very-metal-poor stars by Schuster et al. (1996), and the *uvby–β* data for very-metal-poor stars in Table 1 of Schuster et al. (2004, Paper X). The new *uvby–β* values included in Table 1 were taken during ten observing runs from April 1991 through November 1997.

The *uvby–β* data presented here for the HV stars in Table 1 were taken and reduced using techniques very nearly the same as for SN and SPC; see these previous papers for more details. The four-channel *uvby* section of the SPM photometer is really a spectrograph-photometer that employs exit slots and optical

interference filters to define the bandpasses. The grating angle of this spectrograph-photometer was adjusted at the beginning of each observing run to position the spectra on the exit slots to within about ±1 Å. Whenever possible, extinction-star observations were made nightly over an air-mass interval of at least 0.8 (see Schuster & Parrao 2001; also Schuster et al. 2002), and spaced throughout each night several "drift" stars were observed symmetrically with respect to the local meridian. Using these observations the atmospheric extinction coefficients and time dependences of the night corrections could be obtained for each of the nights of observation (see Grønbech et al. 1976). Finding charts were employed at SPM whenever available. As for previous studies, such as SN and SPC, the program stars were observed at SPM to at least 50 000 counts in all four channels of *uvby* and to at least 30 000 counts for the two channels of Hβ. For all program stars the sky was measured until its contributing error was equal to or less than the error of the stellar count. At SPM an attempt was made to obtain three or more independent *uvby* observations for each of the program stars, and at least five independent observations for those with [Fe/H] ≤ -2.00.

As for the SN and SPC catalogues, all of these data reductions were carried out following the precepts of Grønbech et al. (1976) using computer programs kindly loaned by T. Andersen (see Parrao et al. 1988). At SPM the *uvby–β* standard stars observed were taken from the same lists as for the previous catalogues; these are mostly secondary standards from the catalogues of Olsen (1983, 1984). The reduction programs create a single instrumental photometric system for each observing run, including nightly atmospheric extinctions and night corrections with linear time dependences. Then transformation equations from the instrumental to the standard systems of V, $(b–y)$, m_1, c_1, and β are obtained using all standard stars observed during that observing period. The equations for the transformation to the standard *uvby–β* system are the linear ones of Crawford & Barnes (1970) and of Crawford & Mander (1966). Small linear terms in $(b-y)$ are included in the standard transformation equations for m_1 and c_1 to correct for bandwidth effects in the v filter. Our y measures were transformed onto the V system of Johnson et al. (1966).

For the SPM *uvby–β* data of Table 1, typical (median) values for the standard deviations of a single observation are $\pm 0\overset{m}{.}008$, $0\overset{m}{.}005$–6, $0\overset{m}{.}007$–8, $0\overset{m}{.}008$–9 and $0\overset{m}{.}008$ for V, $(b–y)$, m_1, c_1 and β, respectively.

2.3. The catalogues of observations

Table 1 presents the *uvby–β* catalogue for the 442 HV stars observed at SPM. Column 1 lists the stellar identifications according to several different nomenclatures, mainly DM numbers, NLTT (Luyten 1979a), and the Lowell proper-motion survey (Giclas et al. 1959, 1961, ..., 1975); Col. 2, the V magnitude on the standard Johnson UBV system; and Cols. 3–5 and 7, the indices $(b–y)$, m_1, c_1 and β on the standard systems of Olsen (1983, 1984), which are essentially the systems of Crawford & Barnes (1970) and Crawford & Mander (1966) but with a careful extension to metal-poor stars and with north-south systematic differences corrected. Columns 6 and 8 give N_u and N_β, the total numbers of independent *uvby* and β observations. Stars marked with an asterisk, "*", in the last column have observing notes and cross-identifications in the "Notes" section following the main table, as described in the next paragraphs.

In the second section of Table 1 notes for the HV stars, taken during the observations or during the data reduction and analysis, are given; also listed are many cross-identifications, especially from the HD, DM, LTT (Luyten 1957, 1961), LHS (Luyten 1979b), and Lowell proper-motion catalogues. Many of the observing notes concern the photometric contamination, or possible contamination, by a fainter nearby star, as indicated by a note "D" indicating duplicity. For example, LP808-022 was observed in a very crowded field with a 20 arcsec diaphragm; probably its "star" and "sky" measures were contaminated by fainter nearby stars, and the note "D" plus the accompanying text indicate this problem. LP811-024 and LP866-018 were also observed in crowded fields, as their texts indicate. For LP920-024 the "D" and text show that it was observed with a fainter star located just outside the diaphragm; the contamination is probably very small, due to scattered light from this fainter star. The star G006-013 was observed slightly off-center in the diaphragm to place a faint star just outside the diaphragm; since the bandpasses of the SPM photometer are mainly filter-defined, this small offset should produce negligible errors for the indices. G096-001 was observed with a second star within the diaphragm; in this case the photometric contamination is clear.

The notes "SN" and "SPC" mark those stars which have been repeated from these two previous *uvby–β* catalogues; these are the stars plotted in Figs. 1 and 2, and the values of Table 1 combine the newer *uvby–β* observations with the older. Four stars (+39:2173 = G115–034, +34:0796 = GC4849, +26:2621 = G166–054, and −15:2546 = HD 74000) were sent to us by different astronomers to obtain *uvby–β* data using these different identification numbers, and were observed by us as separate stars until the cross-identifications were checked; *all* the independent observations for each of these four stars have been combined for the values of Table 1, but these stars appear twice in Table 1 using both of the original identifications sent to us, plus the note "repeated". The note "ID?" appears for those stars identified only from their coordinates, without any finding chart. The text "Need confirming observations" marks stars observed only once for the values of Table 1. For these last two categories, "ID?" and "Need ...", the values of Table 1 generally show clear evidence of low photometric metallicities, i.e. low m_1 values for the corresponding $(b–y)$, indicating that the correct HV stars have indeed been observed.

Stars with "++ Red subgiant/giant", such as LP685–047 and G013–050, have $(b–y) \geq 0\overset{m}{.}50$ and $c_1 \geq 0\overset{m}{.}35$; as discussed in SN, the m_1 and c_1 values of these stars may be less accurate, due to non-linearity of the photometric transformations, and the m_1 and c_1 values in Table 1 have been placed in parentheses for such stars. Stars with $(b–y)$ and c_1 values close to these limits, but not both exceeding, have a note of "+", such as LP920–024 and G012–022.

For the cross-identifications, some of the stars from the Lowell-proper-motion survey (the "G" stars) have been

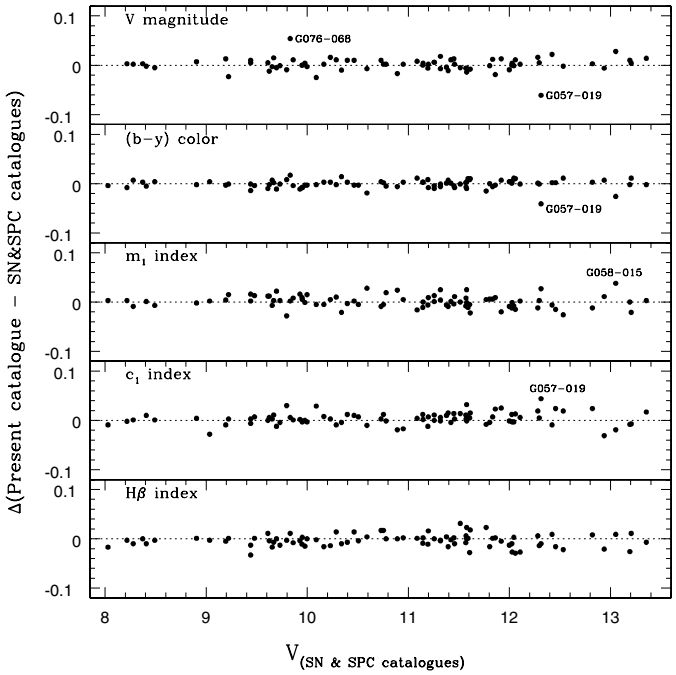

Fig. 1. Comparison of the new *uvby–β* data, taken for the present catalogue, with previous values published in the SN and SPC catalogues, for those 90 stars which have been repeated. The comparison is shown in the sense: the difference between the newer values minus the older values of SN and/or SPC as a function of the previous V magnitudes. The dotted lines show the zero-difference levels, and for three of the stars which are possible photometric variables ($\Delta \geq 0\overset{m}{.}04$), their points have been labeled with their identification numbers.

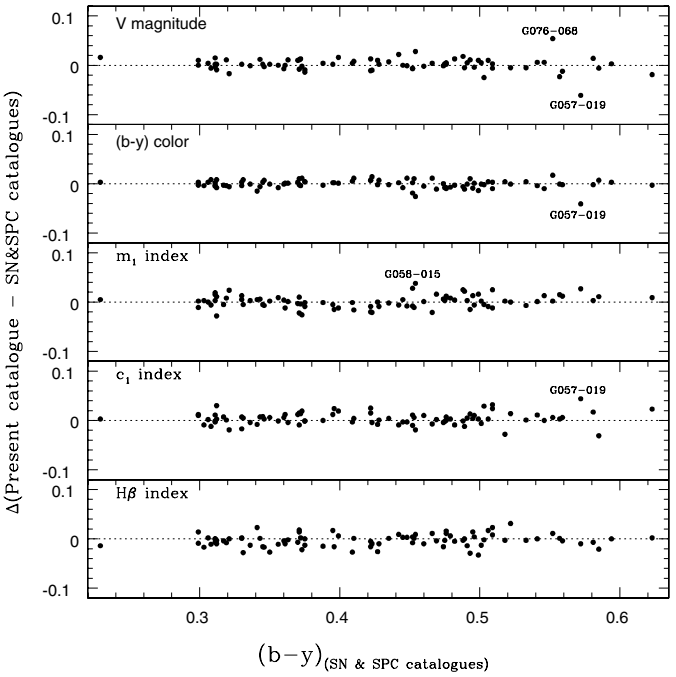

Fig. 2. Same as the previous figure, but as a function of the (b–y) values of SN and/or SPC.

identified in several fields, as many as five in some cases. We give a maximum of two "G" identifiers for each star, and if a given star has more, the second is followed by an ellipsis ("G166–054...", for example).

2.4. Comparisons with our previous photometric catalogues

For 90 of the stars in Table 1, new *uvby–β* observations have been taken for the present catalogue, as well as their older observations presented in the SN and SPC catalogues. These stars are marked in the "Notes" section of Table 1 with "SN" or "SPC". Comparisons of this newer and older *uvby–β* data are shown in Figs. 1 and 2: in Fig. 1 as a function of the older V magnitudes, and in Fig. 2 as a function of the older (b–y) colors. In these figures it is seen that the quality of the newer *uvby–β* data is quite good and closely on the same photometric systems as the older catalogues of SN and SPC. Only a few of the new observations have residuals greater than $0\overset{m}{.}04$ compared to the older values, and these cases have been labeled with the stars' names in Figs. 1 and 2, as candidates for variable stars. The label "G057–019" appears thrice, and "G058–015" and ''G076–068" once each.

The average difference for the comparison of the V magnitudes in Figs. 1 and 2 is +0.0024 with a scatter of ±0.0116; for the (b–y) color, -0.0005 ± 0.0074; for the m_1 index, $+0.0010 \pm 0.0124$; for c_1, $+0.0034 \pm 0.0118$; and for Hβ, -0.0033 ± 0.0126.

3. Reddening, abundances, distances, and classifications

3.1. Interstellar reddening

These stars can be dereddened using the intrinsic-color calibration of Paper II when a value has been observed for Hβ, as for most of the HV stars. This calibration, plus a small offset correction as noted by Nissen (1994)[1], has been used to estimate interstellar reddenings for the 442 high-velocity and metal-poor stars studied here (and also those stars from the SN and SPC catalogues). In Paper X (Fig. 3) a comparison of the interstellar reddenings from this calibration are compared to values derived from the maps of Schlegel et al. (1998). This comparison is quite satisfactory with no evidence for systematic differences. In this paper, reddening corrections from our intrinsic-color calibration have been applied to the *uvby* photometry only when $E(b\text{–}y) \geq 0\overset{m}{.}015$; values smaller than this are mostly not real but are due to the photometric observational errors (see Nissen 1994). For the other reddening corrections, these relations have been used: $A_V = 4.3E(b\text{–}y)$, $E(m_1) = -0.3E(b\text{–}y)$ and $E(c_1) = +0.2E(b\text{–}y)$ (Strömgren 1966; Crawford 1975).

3.2. Photometric stellar abundances

The metallicities, [Fe/H] values, used in this study have been derived from the empirical calibrations of Paper II, one for

[1] Nissen compared Na I column densities from interstellar Na I lines with the color excesses derived from Strömgren photometry plus the intrinsic-color calibration. For 23 stars without detectable interstellar Na I lines the mean value of $E(b\text{–}y)$ was slightly positive, +0.005, suggesting that the zero-point in the $(b\text{–}y)_0$-β calibration of Paper II should be increased by 0.005 mag.

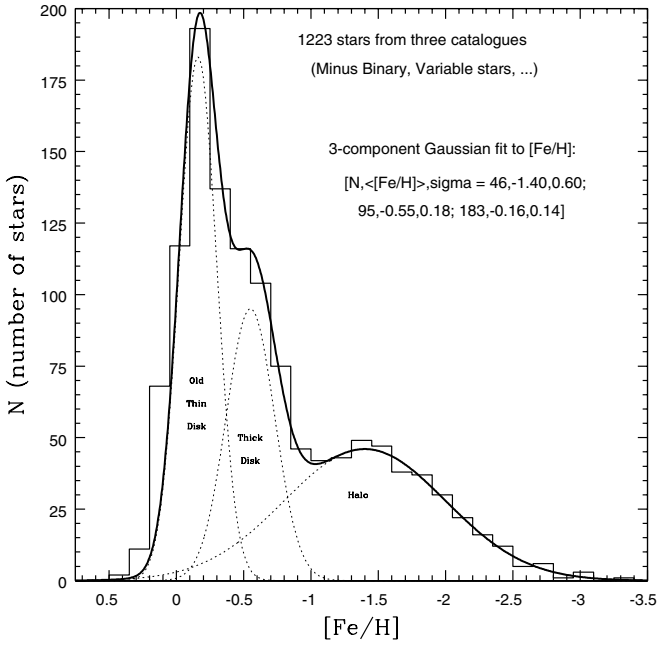

Fig. 3. The [Fe/H] histogram for our total sample of 1223 stars, cleaned of binary and variable stars as described in the text. The [Fe/H] values have been derived from the calibration of Paper II, and the bin size is 0.15 dex. A three-component Gaussian fit to this histogram has been made using mean values and dispersions from the literature for the halo, thick disk, and old thin disk, such as those values from SPC.

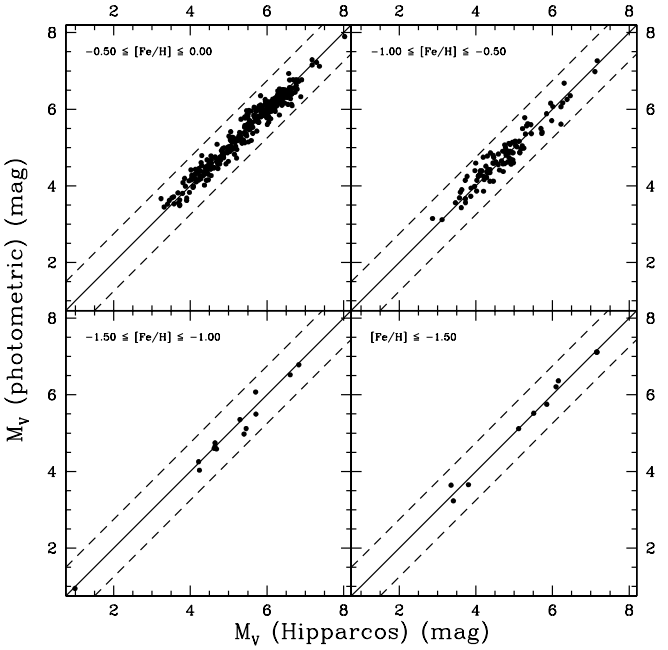

Fig. 4. M_V values (photometric and Hipparcos) are compared for four metallicity intervals: M_V calculated using *uvby* photometry plus our empirical, Hipparcos-based, photometric calibration are plotted against M_V taken directly from the Hipparcos parallaxes. The solid, diagonal lines show one-to-one relations, and the dashed lines show displacements of three-quarters of a magnitude. The [Fe/H] values have been taken from the calibration of Paper II.

F-stars and one for G-stars. The reader is referred to this earlier paper for more details. For these empirical calibrations the estimated standard deviations of a single photometric determination of [Fe/H] are ±0.14 at [Fe/H] ≈ −0.5, ±0.21 at [Fe/H] ≈ −1.5, and ±0.30 at [Fe/H] ≈ −2.5. Comparisons by Feltzing et al. (2001) of photometric abundances using our calibration equations with abundances from two recent spectroscopic studies have shown that these error estimates are overly conservative; they find a scatter of ±0.10–0.11 for the more metal-rich group. Twarog et al. (2002) suggest a systematic error in our G-star [Fe/H] calibration for [Fe/H] $\gtrsim$ −0.2 and $(b-y) \gtrsim 0.47$, but since the present paper concerns only the ages of "turn-off" thick-disk and halo stars (i.e. the bluer stars) with [Fe/H] < −0.2, this possible systematic difference contributes no problem to the following analyses and conclusions. Also, the comparisons of Feltzing et al. (2001) for stars with $-1.0 \lesssim$ [Fe/H] $\lesssim$ +0.3 show systematic differences of our photometric [Fe/H] values of only +0.01–0.02, when compared to the recent spectroscopic studies in the sense $[Fe/H]_{Phot} - [Fe/H]_{Sp}$. And, the comparisons of Martell & Smith (2004; Martell & Laughlin 2002) with the results from their even more recent photometric calibrations for [Fe/H] suggest systematic problems with our older calibration equations are smaller (in the absolute value) than 0.027, for stars with $-0.4 \lesssim$ [Fe/H] $\lesssim$ +0.4. Figure 4 of Karataş et al. (2005) also shows very good agreement between our photometric [Fe/H] values and recent spectroscopic ones over the range $-2.0 \lesssim$ [Fe/H] $\lesssim -0.2$.

In Fig. 3 is shown the [Fe/H] histogram for the 1223 high-velocity and metal-poor stars of our total sample, from the SN, SPC, and present catalogues, cleaned of the binary and variable stars as described below. This plot is very similar to Fig. 1b of SPC. The [Fe/H] histogram is fit very well with three Gaussian components corresponding to the old thin disk, thick disk and halo, with the mean values and widths selected from the literature, especially SPC and Mihalas & Binney (1981). The values used in Fig. 3 are $(\langle[Fe/H]\rangle, \sigma_{[Fe/H]}) = (-1.40, 0.60)$ for the halo Gaussian, (−0.55, 0.18) for the thick disk, and (−0.16, 0.14) for the old thin disk. As noted in SPC, the third component, the thick disk, is very much needed for a good Gaussian fit to this [Fe/H] histogram.

3.3. Absolute magnitudes and distances

The absolute magnitudes and distances for this study are calculated directly from the Hipparcos (ESA 1997) parallaxes when these have errors of 10% or less. When these errors are larger or the stars not found in Hipparcos, the M_V and photometric distances are derived from an empirical calibration based upon Hipparcos data (ESA 1997), described below and previously in Paper X. For stars lying outside the range of this empirical calibration, Hipparcos parallaxes with errors larger than 10% or absolute magnitudes from the older calibration of Paper V are also used to obtain distances. In the analyses to follow, of the 1533 stars with complete kinematic data, only 24 have had their distances derived from these last two, less exact, sources: 7 from Hipparcos with errors greater than 10% and 17 from the older calibration of Paper V.

Our empirical calibration equation for M_V is based upon 512 stars from the Hipparcos data base with parallax errors of

10% or less. The Lutz-Kelker corrections to M_V for these stars are less than about $0\overset{m}{.}12$ (Lutz & Kelker 1973). This sample has been cleaned of binaries using other data bases (principally Dommanget & Nys (1994) from SIMBAD; see Sect. 5 for further details on the cleansing of binaries) and also by an iterative procedure whereby stars with residuals $\gtrsim 0\overset{m}{.}7$ in the calibration comparison have been removed. The calibration equation is a polynomial in $(b–y)$, c_0 and m_0 and higher-order terms to the fourth order. As for the calibrations of Paper II, the solution has been iterated until all terms have T-ratios with absolute values greater than 3. That is, all coefficients are at least three times their estimated errors according to the IDL REGRESS routine (the returned errors of the coefficients are standard deviations). The data have ~500 degrees of freedom and so all coefficients are non-zero at a significance level greater than 0.995. The final regression equation shows a scatter of $\pm 0\overset{m}{.}206$ in M_V. The 512 calibration stars have the following ranges: $-2.4 \lesssim$ [Fe/H] $\lesssim +0.4$, $0\overset{m}{.}038 \leq m_0 \leq 0\overset{m}{.}593$, $0\overset{m}{.}279 \leq (b–y) \leq 0\overset{m}{.}600$, $0\overset{m}{.}102 \leq c_0 \leq 0\overset{m}{.}474$ and $0\overset{m}{.}991 \leq M_V \leq 8\overset{m}{.}029$. The actual region in the $(b–y)$, M_V diagram over which this calibration is well-defined is a somewhat irregular polygon and not a rectangle; it is good for main-sequence, evolving-main-sequence, and turn-off stars over the range in $(b–y)$ given above, and for subgiant stars to $(b–y)$, $M_V \approx (0.42, +0.5)$ and $\approx(0.52, +4.0)$. As mentioned in previous papers, for the most metal-poor stars many photometric calibrations are not entirely adequate since few good calibration stars with [Fe/H] < -2.0 exist. This caveat also applies here, but this Hipparcos-based photometric calibration seems to work quite well for the very metal-poor stars as shown in Paper X of this series. It certainly works very well to [Fe/H] ≈ -2.40, which is the approximate metal-poor limit of the stars analyzed in this paper.

In Fig. 4, M_V values calculated using our Hipparcos-based, empirical calibration are plotted against M_V derived directly from the Hipparcos parallaxes for four metallicity intervals: $-0.50 \leq$ [Fe/H] ≤ 0.00, $-1.00 \leq$ [Fe/H] ≤ -0.50, $-1.50 \leq$ [Fe/H] ≤ -1.00, and [Fe/H] ≤ -1.50, according to the photometric [Fe/H] calibration of Paper II. The nine stars of the last panel have [Fe/H] values in the range $-2.39 \leq$ [Fe/H] ≤ -1.57, are the same stars plotted in Fig. 7 of Paper X, and show that our calibration stars do not extend to the lowest [Fe/H] values of some of the HV stars, but do cover well the metallicities of the isochrones used in this publication. The agreement seen in Fig. 4 is quite satisfactory for all four panels.

In the analyses to follow, three different symbols are used to denote the M_Vs and distances with different sources and qualities. Stars with values direct from Hipparcos with errors less than 10% are shown as circles, those with values from the empirical, IDL-Hipparcos photometric calibration, as squares, and those from the older calibration of Paper V or from Hipparcos but with larger errors, as triangles.

3.4. The $(b–y)_0$, c_0 diagram and photometric classifications

In Fig. 6 of Paper X a $(b–y)_0$, c_0 diagram is presented for very-metal-poor (VMP) stars, and a scheme is suggested for classifying these VMP stars into categories such as those identified in globular cluster CM diagrams: turnoff stars (TO), main sequence stars (MS), blue stragglers (BS), the transition from blue-straggler to turnoff (BS-TO), subgiant stars (SG), red giants (RG), horizontal branch stars (HB), the transition red-horizontal-branch to asymptotic-giant-branch (RHB-AGB), blue horizontal branch (BHB), subluminous stars (SL), and the transition from the blue-horizontal-branch to subluminous (SL-BHB). This scheme is also useful for classifying the evolutionary states of stars from the present paper, as well as stars from the SN and SPC catalogues. However, the stars in Fig. 6 of Paper X have a mean metallicity of [Fe/H] ≈ -2.4, and the stars studied here range from above-solar [Fe/H] values to [Fe/H] ≈ -5.0. To adjust for a possible systematic error in the photometric classifications, the c_0 values of the stars have been corrected according to their [Fe/H] and $(b–y)_0$ values using Eq. (2) of Paper V to obtain c_0 values corresponding to [Fe/H] $= -2.40$. According to Paper V, this Eq. (2) is valid only over the range $+0.27 \lesssim (b–y)_0 \lesssim +0.58$. The corrections applied to c_0 are small; the median of the absolute values is ≈0.050, and the mean ≈0.064, excluding the two stars in Table 2 with a Note of "B", indicating a very uncertain value for [Fe/H]. (A very small shift in the $(b–y)_0$ values, due to the metallicity differences, has been ignored here.) Also, according to Paper II, the stars' photometric [Fe/H] values have been derived only over the range $+0.22 \lesssim (b–y)_0 \lesssim +0.60$, and for stars not too evolved: $+0.17 \lesssim c_0 \lesssim +0.60$ for the F-stars and $+0.10 \lesssim c_0 \leq +0.50$ for the G-stars. Stars outside these ranges have not had their c_0 values corrected to [Fe/H] $= -2.40$ prior to the photometric classification. Also from Paper II, the intrinsic-color calibration is useful only over the ranges, $+0.25 \lesssim (b–y)_0 \lesssim +0.55$ and $+0.12 \lesssim c_0 \lesssim +0.54$; for stars outside these ranges, c_0 and $(b–y)_0$ have been set equal to their observed values, c_1 and $(b–y)$.

According to these corrections, color limits, and Fig. 6 of Paper X, most of the stars in SN, SPC, and this paper classify as main sequence (MS) and turnoff (TO) stars. (In Fig. 6 of Paper X the line separating the MS and SL stars was very roughly drawn employing only a small number of stars, ≈10; for the present work a much larger sample of stars has shown the need to shift this line downward by about $0\overset{m}{.}00$ at $(b–y)_0 = 0.30$, $0\overset{m}{.}10$ at $(b–y)_0 = 0.40$, and $0\overset{m}{.}06$ at $(b–y)_0 = 0.50$; with this shift the distinction between MS and SL is clear.) In Table 2 are given those stars *not* classified as MS or TO: in Col. 1 is shown the stars' identification numbers; Cols. 2 and 3, the $(b–y)_0$ and c_0 values, respectively; Col. 4, the photometric [Fe/H] value; Col. 5, the photometric classification from Fig. 6 of Paper X; and Col. 6, notes. In this latter "Notes" column, "A" emphasizes stars without photometrically determined [Fe/H] values; "B" marks two stars with [Fe/H] ≈ -5.0 (at such low values the m_1 index is no longer sensitive to the metallicity, and so these [Fe/H] values are very uncertain); "C" shows two red giant stars with $(b–y) \geq +0.50$ and $c_1 \geq +0.35$ (as discussed in SN, such stars will have less accurate c_1 values due to transformation errors); and "D" indicates stars which are repeated in this table (4306 = HD 4306, 25532 = HD 25532, G014–032 = G014–032, W5793 = −12:2669, and W6296 = +44:1910).

These stars of Table 2 represent the redder, bluer, and/or more evolved stars of our total sample and are interesting for future studies, such as spectroscopic ones. Many of these stars fall outside the photometric calibrations and their color-limits, as discussed above and as can be seen in the fourth column, where many photometric [Fe/H] values are missing. So in general the classifications are rough, but do serve to point out the more extreme, potentially interesting stars of our sample. For example, six stars have been classified "SL" (HD 26, G038–001, HD 108754, G015–024, G152–035, and 833–020), are photometrically unusual, and are candidates for being subluminous, i.e. degenerate stars. Twelve stars are candidate subgiant stars: HD 17072, −24:1782, W6296 = +44:1910, HD 103459, HD 128204, HD 140283, HD 165271, HD 200654, G092–006, G026–012, 811–024, and G170–047. Another 24 stars are potentially even more evolved with eight red-giant classifications, nine horizontal-branch candidates, four RHB-AGBs (HD 25532, HD 117327, HD 229274, and HD 195636), and three BHBs (HD 139961, HD 213468, and HD 214539). Nine of the bluer stars are possible blue stragglers with "BS" or "BS-TO" classifications.

4. Kinematic data and galactic velocities

4.1. Proper motions and radial velocities

The proper motions and coordinates used in this paper have been taken primarily from three sources: Hipparcos (ESA 1997), Tycho–2 (Høg et al. 2000), and the revised NLTT (Salim & Gould 2003). For a few stars other sources have been employed, such as the original NLTT (Luyten 1979a), the LHS (Luyten 1979b), the Lowell Proper Motion Survey (Giclas et al. 1959, 1961, ..., 1975), and the PPM Star Catalogue (Röser & Bastian 1991). Of the 1706 stars from our combined three catalogues of photometric data (SN, SPC, and this paper) proper motions have been found for all of the stars except three. In general the proper motion errors range from 0.5–3.0 mas/yr per component for the best sources, such as Hipparcos and Tycho–2, to as large as $\gtrsim$10 mas/yr per component for the other sources, such as the NLTT and the Lowell Proper Motion Survey.

The radial velocities for the present study have been obtained from the literature, from a number of sources, such as Carney et al. (1994), Barbier-Brossat et al. (1994, 2000), Nordström (2000), Ryan & Norris (1991), Fouts & Sandage (1986), and Abt & Biggs (1972). Of the stars from our three photometric catalogues radial velocities have been found for all except 60 stars. The observational errors of these velocities range from a few tenths of a km s^{-1} for the best sources, such as Carney et al. (1994) and Nordström (2000), to $\approx$7 km s^{-1} for the older sources.

4.2. Galactic velocities

There are 1706 stars in our combined three photometric catalogues, of which 90 have been repeated and another 87 are without complete kinematic data, lacking either radial velocities, distances, or proper motions, leaving 1533 stars with complete data for calculating the Galactic velocities, (U, V, W). These velocities and their errors have been derived using the formulae and matrix equations from Johnson & Soderblom (1987). For these calculations, the celestial coordinates, proper motions, and radial velocities, as well as the errors of the proper motions and radial velocities, have been taken from the observational sources and compilations mentioned in the previous subsection.

The stellar distances have been derived from the absolute magnitudes as described above in subsection 3.3: from Hipparcos parallaxes (ESA 1997), from our present photometric M_V calibration, which also depends upon Hipparcos, or from the older photometric M_V calibration of Paper V. The distance errors have been taken from the Hipparcos parallax errors, when appropriate, or, for the newer empirical photometric M_V calibration, set equal to 10% as a conservative estimate; the final regression equation gives a scatter of $\pm 0\overset{\mathrm{m}}{.}206$ for this M_V calibration. For 17 stars with distances from the older calibration of Paper V, the distance errors have been adjusted according to the evolutionary corrections, the δM_V of this previous paper. For example, for stars which are little evolved, $-0\overset{\mathrm{m}}{.}25 < \delta M_V < +0\overset{\mathrm{m}}{.}25$, the distance error has been set at 10%, while for stars very evolved, $\delta M_V > +4\overset{\mathrm{m}}{.}0$, at 30%, with other levels of error in between. This scaling of the distance error with evolutionary status of the star takes into account various systematic problems with this older M_V calibration.

The Galactic velocities from Johnson & Soderblom (1987) correspond to a right-handed coordinate system with (U, V, W) positive in the directions of the Galactic center, Galactic rotation, and the North Galactic Pole, respectively. In the present paper (+10.0, +14.9, +7.7) km s^{-1} have been used to correct (U, V, W) for the solar motion, (U', V', W') = (U, V, W) + (+10.0, +14.9, +7.7), and our typical (median) errors in these velocities are ($\pm$6.2, $\pm$6.6, $\pm$4.8) km s^{-1}.

Tables 3 and 4 show the input and output values for these kinematic calculations, respectively, plus Table 4 also gives other parameters used in the following analyses, such as the dereddened photometry as described in Sect. 3.1, the photometric metallicities from Sect. 3.2, the selected absolute magnitudes from Sect. 3.3, and the X parameter from Sect. 6.1 below. In Table 3 the first two columns give the stars' identifications, where Col. 1 contains our internal numbers and Col. 2 identifications from various external catalogues. In Col. 1, numbers prefixed by "SN" refer to the *uvby–β* catalogue of SN, prefixed by "SPC" the catalogue of SPC, and prefixed by "SPG" the present catalogue of Table 1; in each of these sections of Table 3 the stars are listed in the same order, and in Col. 2 the preferred external identifications are the same, as in those original catalogues: SN, SPC, and Table 1. In Table 3, Cols. 3–5 and 6–8 give the right ascension and declination, Col. 9 the radial velocity in km s^{-1}, Cols. 10 and 11 the proper motions in right ascension and declination (μ_α and μ_δ) in mas yr^{-1}, Cols. 12–14 the standard errors of the radial velocity, of μ_α, and of μ_δ in the same units as above, respectively, Cols. 15–16 the distance in parsecs as described in Sect. 3.3 plus its estimated standard error, and finally in Col. 17 the epoch of these values.

In Table 4 the fist two columns are the same as in Table 3, Cols. 3–5 contain the Galactic velocities (U', V', W') in km s^{-1},

Cols. 6–8 the standard errors of these velocities, respectively, Cols. 9–10 once again the distance in parsecs plus its estimated standard error, Cols. 11–14 the dereddened photometry $(V_0, (b-y)_0, m_0, c_0)$, Col. 15 the photometric metallicity ([Fe/H], where "9.99" indicates that no value has been obtained due to the limits of the calibrations given in Paper II), Col. 16 the selected absolute magnitudes from Sect. 3.3, Col. 17 a code for these absolute magnitudes (where "1" indicates an absolute magnitude derived directly from a Hipparcos parallax with a less than 10% error, "2" an absolute magnitude from the empirical calibration described in Sect. 3.3, and "3" those M_Vs from the older calibration of Paper V or from Hipparcos but with larger relative errors), Col. 18 the values of the X parameter from Sect. 6.1 (where "−999.999" indicates no value since [Fe/H] has not been obtained), and Col. 19 a code for the binary and variable stars, as described in the following section (where "1" indicates a star not identified as a binary, "2" a double-lined spectroscopic binary, SB2 or dlsb, "3" all other binaries, suspected binaries, or those stars noted at the telescope to be contaminated, and "4" the probable photometric variables). Table 4 contains 1533 lines, corresponding to 1533 different stars, less than Table 3, since all repetitions, between or within the different photometric catalogues, have been eliminated.

5. Binary and variable stars

Of the 1533 stars in our kinematic sample, many are known or suspected binary stars, and a few are also known or suspected variable stars. In addition, during the observations of the *uvby–β* photometry it was noted at the telescope that nearby fainter stars produced slight, some, or significant luminous contamination to the data being either just outside the photometer's diaphragm, at the diaphragm's edge, or well within, respectively. These are noted as such in the second half of Table 1 of this paper; the SN and SPC catalogues also have similar "Note" sections to their tables. To correct our sample for the possible errors and systematic effects that such contamination might cause in our final results and conclusions, the sample of 1533 stars with complete kinematic data has been put to several cleansings using the following sources: the observing notes taken at the telescope, the lists and catalogues of Carney (2003) and of Carney et al. (1994), and also the catalogues of data contained in the SIMBAD data base (principally Dommanget & Nys 1994).

The final data base cleaned of all binaries, suspected binaries, stars with contaminated data as seen at the telescope, and probable variable stars contains 1223 high-velocity and metal-poor stars. This sample is seen in Figs. 4–7. However, in some of the other analyses to follow, such as Figs. 8–12, all of the 1533 stars are plotted but with different symbols: open symbols represent the most contaminated binaries, the double-lined spectroscopic binaries (SB2 or dlsb); crossed-open symbols, all other binaries, suspected binaries, or those noted at the telescope to be contaminated; asterisk-open symbols, the probable photometric variables; and solid symbols, stars which suffer none of the above.

This binary-star symbolism is combined with that described above in Sect. 3.3 for the M_Vs and distances, so that, for example, an SB2 star with its parallax taken from Hipparcos with less than a 10% error, is represented in the following figures with an open circle. A non-binary, non-variable star with its distance from the IDL-Hipparcos empirical calibration, as a solid square, and so forth. A more complete description for the total symbolism of the following figures is given in the text to Fig. 8.

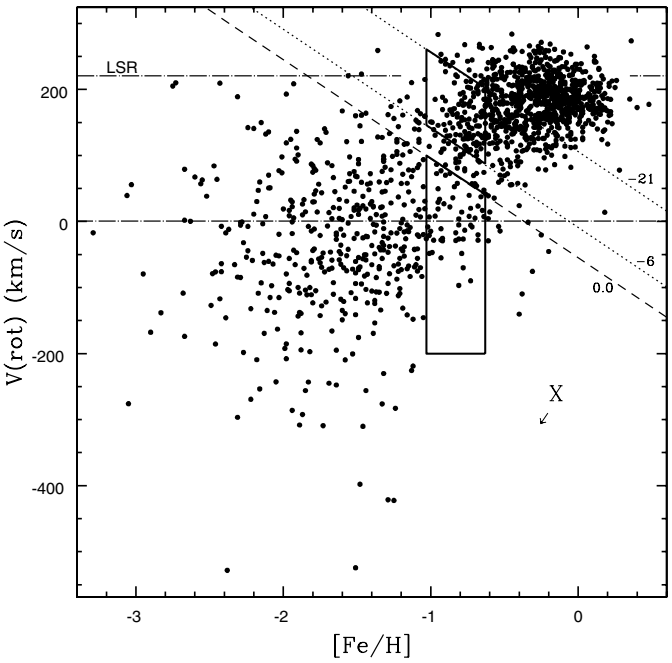

Fig. 5. The [Fe/H], V(rot) diagram for 1223 stars with reliable kinematic parameters, cleaned of binary and variable stars. V(rot) = V' + 220 km s^{-1}, and the [Fe/H] values are from the calibration of Paper II. The dashed diagonal line is that suggested in Paper V to separate halo from "high-velocity disk" stars, and the direction of increasing "X", the stellar-population parameter defined in SPC, is shown. The diagonal dotted lines correspond to X = −6.0 and −21.0, the limits used in this paper to define the "thick disk". The horizontal dash-dot lines show V(rot) = 0 and +220 km s^{-1}, the latter corresponding to the Local Standard of Rest. The two quadrilaterals show examples of samples (in this case for "halo" and "thick-disk" groups with $-1.03 \leq$ [Fe/H] ≤ -0.63) to be compared to isochrones in the $(b–y)_0$, M_V diagram, such as in Fig. 12 below.

6. [Fe/H], *V*(rot) diagram

6.1. Appearance and use

In Fig. 5 a [Fe/H], V(rot) diagram is presented, similar to Fig. 5 of SPC but with more stars, better kinematic data, better distances, and cleaned of the binary and variable stars. For this diagram V(rot) = V' + 220 km s^{-1}, and V' is the Galactic velocity in the direction of Galactic rotation corrected for the solar motion, as described above in Sect. 4.2, $V' = V$ + 14.9 km s^{-1}, and Θ_0 = 220 km s^{-1} is the assumed value of the circular speed of the Milky Way at the solar position (Kerr & Lynden-Bell 1986). [Fe/H] is the photometric metallicity as described in Sect. 3.2. As in SPC, two main stellar components are apparent in this Fig. 5, one centered at [Fe/H], V(rot) ≈ (−0.25, +180 km s^{-1}), and the other, more

dispersed, at [Fe/H], $V(\mathrm{rot}) \approx (-1.5, -25\ \mathrm{km\,s^{-1}})$. The diagonal dashed line labeled "0.0" is that defined and used in Paper V and SPC to separate the halo stars (below and to the left) from the "high-velocity disk" stars (above and to the right). The dot-dash line labeled "LSR" indicates the level in $V(\mathrm{rot})$ of the Local Standard of Rest (220 $\mathrm{kms^{-1}}$), and the other horizontal dot-dash line, $V(\mathrm{rot}) = 0\ \mathrm{km\,s^{-1}}$. Also shown is the direction of increasing X, the stellar population parameter defined in SPC as a linear combination of $V(\mathrm{rot})$ and [Fe/H], and the loci with constant values of $X = -6.0$ and $X = -21.0$, the two diagonal dotted lines labeled with these values. The criterion, $-21.0 \leq X \leq -6.0$, is one of those to be used and discussed in this paper for defining the "thick disk". For example, the two quadrilaterals of Fig. 5 define halo ($X \geq 0.00$) and "thick disk" ($-21.0 \leq X \leq -6.0$) samples, both with $-1.03 \leq$ [Fe/H] ≤ -0.63, to be compared in $(b–y)_0, M_V$ diagrams for studying their relative ages. In general stars with more positive values of X are more halo-like, and stars with more negative values, more disk-like. As shown in SPC and in Fig. 6, the dashed line $X = 0.00$ provides a fairly good, but not totally clean, separation of the halo and disk stars; the "halo" sample, below and to the right in Fig. 5, *is* a nearly clean sample, largely free of other stellar populations, while the "high-velocity disk" stars, above and to the right, are a mixture of thick-disk, old-thin-disk, and halo stars. This X parameter shown in Fig. 5 has been used previously, such as in SPC and MS, to separate several stellar populations and Galactic components and to study their relative-age differences.

The discriminant X is useful for separating the stellar populations, but probability algorithms given in the literature by Bensby et al. 2003 and by Venn et al. 2004 may be superior. In these, the stars' (U, V, W) velocity information is compared to the Galactic Gaussian velocity-ellipsoid components, with assumptions concerning the velocity dispersions and asymmetric drifts of the thin disk, thick disk, and halo, in order to estimate for each star its probability of membership in each of these populations. Metallicity information, [Fe/H] or [m/H], is not used by these alternate methods. The effectiveness of our X criterion for separating out thick-disk stars has been discussed and shown in Karataş et al. (2005).

6.2. Histogram against X

In Fig. 6 a histogram against X is presented, similar to Fig. 8b of SPC, with a bin size of three units in X. That is, the stars are counted in diagonal slices parallel to the dashed line of Fig. 5 with intervals of three in X. Again, a Gaussian fit to the histogram has been attempted with three components, corresponding to the halo, thick disk, and old thin disk. Figure 6 shows one of our better fits with the normalization, mean value, and width of $(N, \langle X\rangle, \sigma_X) = (26, 23.0, 19.0)$ for the halo component, $(60, -18.0, 8.0)$ for the thick disk, and $(122, -29.0, 3.8)$ for the old thin disk[2]. Clearly this Gaussian fit to the histogram is not as good as that seen in Fig. 3 for the [Fe/H] histogram, nor as good as the Gaussian fit to the X histogram presented in Fig. 8b of SPC. The intermediate "thick-disk" Gaussian does not fit well the data, and there seems to be indications for two "thick-disk" components, one as a shoulder to the halo distribution with $X \approx -8$, and the other as a shoulder to the old thin disk with $X \approx -20$. The sharp drop in the histogram at $X = -15$ is quite robust, showing up also in the histogram for the total sample of 1533 stars and in the various cleansings of the binary and variable stars.

6.3. Two groupings in the thick disk?

In Fig. 7 contour plots of the [Fe/H], $V(\mathrm{rot})$ diagram are given, in the upper panel for the entire figure, and in the lower panel concentrating more on the "high-velocity-disk" stars at the more positive values of [Fe/H] and $V(\mathrm{rot})$, i.e. more negative values of X, as shown by the labels on the diagonal dotted lines. In the upper panel a kernel with a size of (0.40 dex, 60 $\mathrm{km\,s^{-1}}$) and a step size of (0.20 dex, 30 $\mathrm{km\,s^{-1}}$) has been used to sum over the [Fe/H], $V(\mathrm{rot})$ diagram, and 100 levels of contour plotted; in the lower panel a kernel with a size of (0.20 dex, 30 $\mathrm{km\,s^{-1}}$), step size of (0.10 dex, 15 $\mathrm{km\,s^{-1}}$), and 40 contour levels. In the upper panel, one can appreciate well again the two large, overall components mentioned above for Fig. 5, the halo population centered at [Fe/H], $V(\mathrm{rot}) \approx$ (−1.3 dex, −40 $\mathrm{km\,s^{-1}}$), and a disk component at [Fe/H], $V(\mathrm{rot}) \approx$ (−0.2 dex, +185 $\mathrm{km\,s^{-1}}$). It appears that the median halo undergoes retrograde rotation in the Galaxy, assuming $\Theta_0 = 220\ \mathrm{km\,s^{-1}}$ for the circular speed of the Milky Way at the solar circle; if a more modern value for this circular speed is used, such as the value of $\Theta_0 = 234 \pm 13\ \mathrm{km\,s^{-1}}$ from Fukugita & Peebles (2004), the median halo still remains retrograde at about the two-sigma level.

The lower panel of Fig. 7 shows evidence of additional structure, i.e. stellar components, for the "high-velocity-disk" stars, $X < 0.00$. The main peak at [Fe/H], $V(\mathrm{rot}) \approx$ (−0.2 dex, +185 $\mathrm{km\,s^{-1}}$) corresponds to the old thin disk stars, but two other components are noted with [Fe/H], $V(\mathrm{rot}) \approx$ (−0.4 dex, +160 $\mathrm{km\,s^{-1}}$) and [Fe/H], $V(\mathrm{rot}) \approx$ (−0.7 dex, +120 $\mathrm{km\,s^{-1}}$). The division between these two latter groups gives the sharp drop at $X = -15$ in the X histogram of Fig. 6. In other words, what was called the "thick disk" in previous papers may have two components. To check that these two components really are "thick", the dispersions in the vertical Galactic velocity W' have been examined. For the more disk-like component, its limits have been set at $-23.0 \leq X \leq -16.0$ and $-0.60 \leq$ [Fe/H] ≤ -0.20; its vertical dispersion in the W' velocity is 45.2 $\mathrm{km\,s^{-1}}$ from 146 stars drawn from the total sample of 1533 stars, and 45.8 $\mathrm{km\,s^{-1}}$ for 125 stars drawn from the cleaned sample of 1223. For the more halo-like component, its limits have been taken at $-14.0 \leq X \leq -6.0$ and

[2] The ratios of these normalizations do not reflect the local population densities of the halo, thick disk, and old thin disk, but have been clearly biased by the largely kinematic selection criteria of our sample; this is also true for the normalizations of Fig. 3. Previous studies have generally shown a local space density for the halo of 0.1–0.5%, and for the thick disk of 2–11%, relative to the thin disk (for example, Gilmore 1984; Robin & Crézé 1986; Sandage 1987; Yamagata & Yoshii 1992; Reid & Majewski 1993; Kerber et al. 2001; Larsen & Humphreys 2003; Karaali et al. 2004).

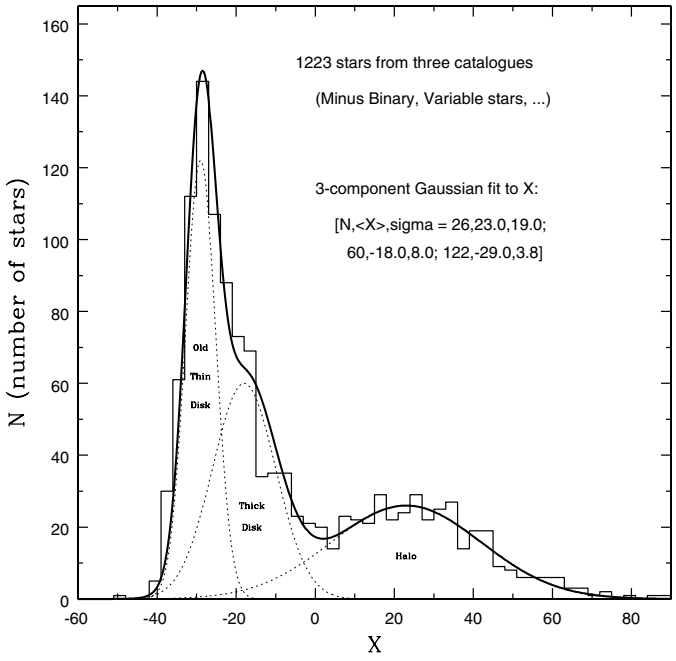

Fig. 6. Histogram against X, the stellar-population parameter defined in Paper VI and shown in the previous figure. Our total, cleaned sample of 1223 stars is included in this histogram. A three-component Gaussian fit has been attempted taking mean values and dispersions from the literature for the halo, thick disk, and old thin disk. With the improved kinematics and photometric distances of this paper, the Gaussian fit to the intermediate "thick-disk" X-values, $-21 \lesssim X \lesssim -6$, is not nearly as good as it was in Fig. 8b of SPC; there is now a serious discrepancy, a sharp drop in the counts, at $X \approx -15$.

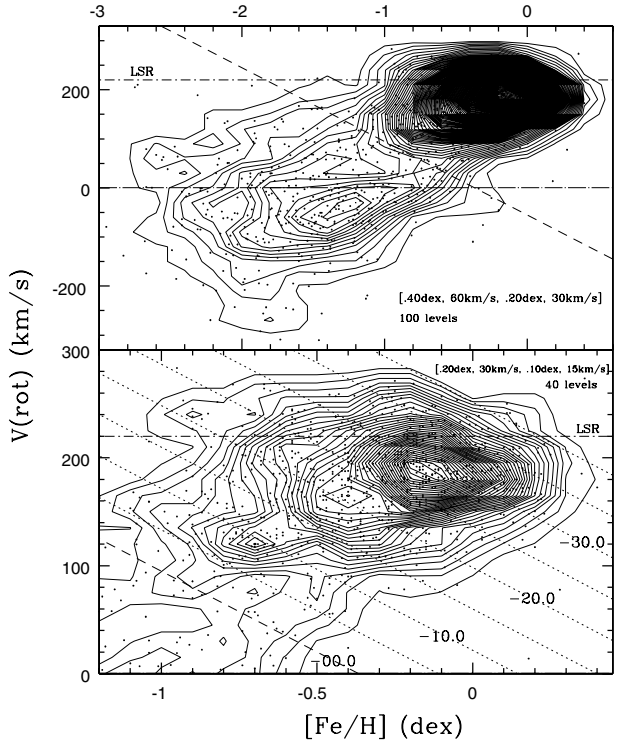

Fig. 7. [Fe/H], V(rot) contours produced by passing a kernel over the full extent of the 1223 high-velocity and metal-poor stars, which are also plotted as small points. In the upper panel, the kernel size was (0.40 dex, 60 km s^{-1}) with a step size of (0.20 dex, 30 km s^{-1}), and in the lower a kernel of (0.20 dex, 30 km s^{-1}) with a step size of (0.10 dex, 15 km s^{-1}). In the upper panel 100 equal-spaced levels have been shown over nearly the full extent of the halo and "high-velocity disk" stars, with only the sparsest regions not included by a contour. The lower panel shows an expanded view of the "high-velocity disk" region with 40 equal-spaced levels. The horizontal short-dash–dot line shows the V(rot) = 220 km s^{-1} value of the Local Standard of Rest (LSR); the horizontal long-dash–dot line, V(rot) = 0 km s^{-1}; the diagonal dashed line, the loci of $X = 0.00$, suggested in Paper V to separate halo from "high-velocity disk" stars; and the diagonal dotted lines the loci with constant X values of $-5.0, -10.0, -15.0, -20.0$, ..., as labeled.

$-0.90 \leq$ [Fe/H] ≤ -0.50; its vertical dispersion is 61.3 km s^{-1} from 83 stars drawn from the total sample, and 62.0 km s^{-1} for 64 stars from the cleaned sample. These dispersions for the more halo-like, thick-disk component are probably contaminated by halo stars, as can be seen in the Gaussian fit of Fig. 6, but these dispersions do clearly show that these two thick-disk components really are "thick" and not just physical extensions of the old thin disk; SPC and MS argued that the maximum possible vertical dispersion for the old thin disk lies in the range 30–35 km s^{-1}, based on works such as that of Wielen (1977) or Freeman (1991).

7. $(b–y)_0$, M_V diagrams and stellar ages

7.1. The thick disk

In Fig. 8 are given $(b–y)_0$, M_V diagrams for the two proposed components of the thick disk, one with $-23.0 \leq X \leq -16.0$ and $-0.60 \leq$ [Fe/H] ≤ -0.20 (the more disk-like), and the other with $-14.0 \leq X \leq -6.0$ and $-0.90 \leq$ [Fe/H] ≤ -0.50 (the more halo-like). The M_V values have been derived as described above in Sect. 3.3, from Hipparcos, from our empirical photometric calibration, and from the older calibration of Paper V[3]. The $(b–y)_0$ values have been dereddened as described in Sect. 3.1. The isochrones are those of Bergbusch & VandenBerg (2001) as transformed to *uvby* photometry by Clem et al. (2004). In the upper panel the isochrones corresponding to [Fe/H] = −0.40 and [α/Fe] = +0.00 have been plotted, and in the lower, [Fe/H] = −0.70 and [α/Fe] = +0.30. These [α/Fe] values seem most appropriate considering the mean relation between [α/Fe] and [Fe/H] seen in field stars for [Fe/H] > −1.0 (Márquez 2004; Bressan 2004; Barbuy et al. 2003; Clementini et al. 1999; McWilliam 1997). The error bars correspond to a 10% distance error and to a typical single observation in $(b–y)$; many of the stars will have errors smaller by a factor of the square root of two or three. The symbols of

[3] Papers by Furhmann (1998), Prochaska et al. (2000), Feltzing et al. (2003), Reddy et al. (2003), Bensby et al. (2003, 2005), and Brewer & Carney (2004) show clearly that the thin disk and thick disk obey different [α/Fe] versus [Fe/H] relations. In as much as the $(b–y)$, m_1, and c_1 photometric indices do not track [α/Fe], this will produce increased scatter in our photometric M_v calibration. However, this difference will not produce systematic effects in our Figs. 8, 12, and 13, since we are comparing only thick-disk, or thick-disk plus halo, stars in these figures.

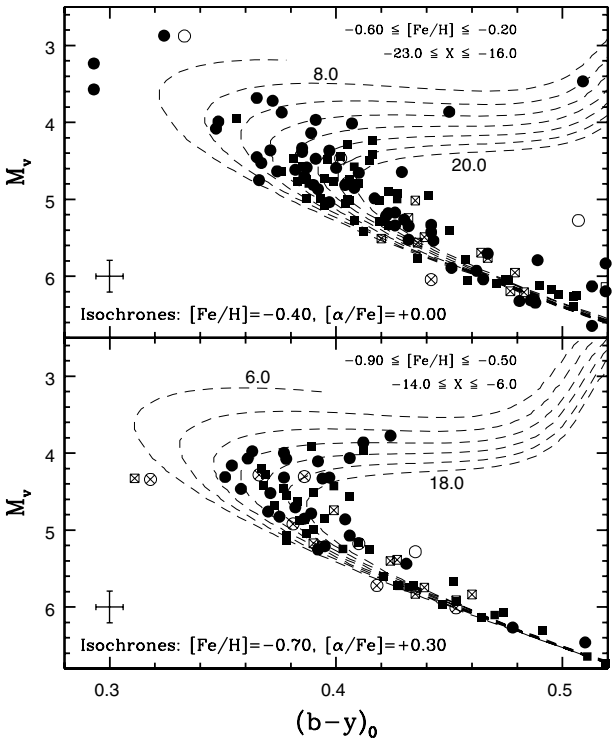

Fig. 8. $(b–y)_0$, M_V diagrams for two of the disk groups identified in the previous figure, one with [Fe/H] ≈ −0.40 and $-23 \lesssim X \lesssim -16$, and the other with [Fe/H] ≈ −0.70 and $-14 \lesssim X \lesssim -6$. Isochrones from Bergbusch & VandenBerg (2001; Clem et al. 2004) are plotted in steps of 2 Gyr from 6 Gyr to 18 or 20 Gyr, and error bars corresponding to a single observation are shown; most of the stars plotted have three or more photometric observations. For the symbols: all circles correspond to M_V values direct from the Hipparcos parallaxes with errors less than 10%; all squares to M_V from our photometric calibration; and all triangles to other quality M_V values, such as from Hipparcos parallaxes with errors larger than 10% or from the calibration of Paper V. All solid symbols show non-binary stars; open symbols, SB2 binaries; crossed-open, other binary stars; and the asterisk-open, the photometrically variable stars.

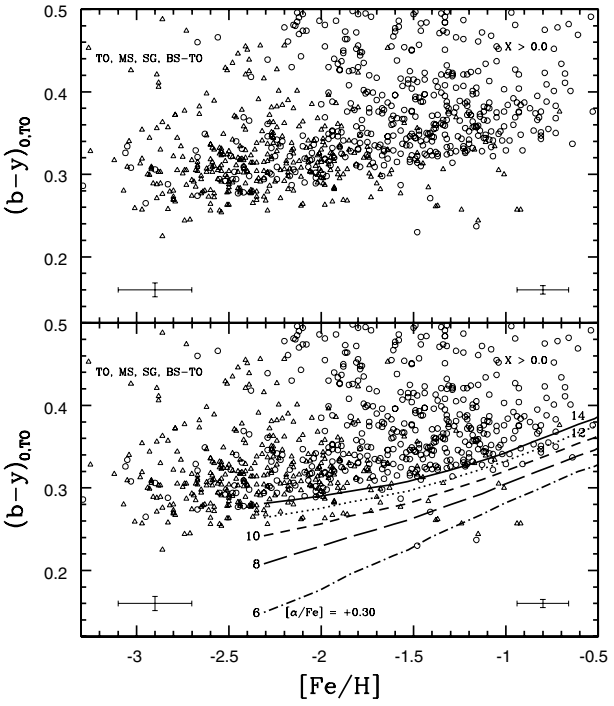

Fig. 9. The [Fe/H], $(b–y)_0$ diagram for the high-velocity and metal-poor stars of this paper (open circles) plus the very-metal-poor stars from Schuster et al. (2004) (open triangles). The [Fe/H] values come from the calibration of Paper II for the former stars, and from calibrations of the HK survey, as described in Schuster et al. (2004), for the latter. The error bars show the calibration errors for [Fe/H], as given in the above sources, and the error of a single observation for $(b–y)_0$; most of the high-velocity and metal-poor stars have been observed three or more times, and the very-metal-poor stars 1–3 times. For the former group only halo stars ($X > 0.0$) have been included, and for the latter group only the turn-off, main-sequence, and subgiant stars (TO, MS, SG, and TO-BS) have been plotted, as classified in Schuster et al. (2004). In the lower panel the turn-off loci from the isochrones of Bergbusch & VandenBerg (2001; Clem et al. 2004) are over-plotted for the ages of 6, 8, 10, 12, and 14 Gyr, with [α/Fe] = +0.30.

Fig. 8 combine the notations for M_V and for the binary/variable stars, as described at the end of Sects. 3.3 and 5, and in the text to the figure; the symbols representing the most reliable data are the solid circles (non-binary, non-variable stars with M_V from Hipparcos, and a less than 10% parallax error), and the solid squares (non-binary, non-variable stars with M_V from our empirical Hipparcos photometric calibration).

In the upper panel of Fig. 8 (the more disk-like component) a wide range of ages is present, as might be expect from Fig. 7. This group lies where there is significant overlap between the thick disk and the old thin disk, with probably a few halo stars thrown in also. A few stars are seen with ages less than 6 Gyr, and some with quite large ages, ≳13 Gyr, but the most obvious sequence is defined for a group of 8–10 stars with ages ≈9–11 Gyr. In the lower panel of Fig. 8 the scatter is much less, and the more obvious sequence corresponds to an age ≈11–14 Gyr. Below in Fig. 13, it will be seen that the halo population of the Galaxy has a mean age of 13.0 ± 0.2 Gyr. So, the lower panel of Fig. 8 shows that part of the thick disk has an age very similar to that of the halo. Such a conclusion has already been obtained by MS using field stars, and by Venn et al. (2005), who use globular clusters with measured space velocities to assign memberships in either the halo or thick disk, finding similar ages for the two cluster groups and, hence, for the two populations. Also, Fig. 8 shows that the two components of the thick disk of Figs. 6–7 have ages differing by about 2.5 Gyr.

7.2. Younger metal-poor stars?

In Fig. 9 a [Fe/H], $(b–y)_0$ diagram is plotted, similar to Fig. 11 of Schuster et al. (1996) but with more stars and better, more recent isochrones, those of Bergbusch & VandenBerg (2001; Clem et al. 2004) In the upper panel only the stars and error bars are plotted without the isochrones. The error bars correspond to typical errors in [Fe/H] and in $(b–y)_0$ at the more metal-rich and more metal-poor limits of this figure. The open circles mark the halo stars ($X > 0.00$) from the SN, SPC, and present catalogues of high-velocity and metal-poor stars. The open triangles show the VMP stars from Paper X and from

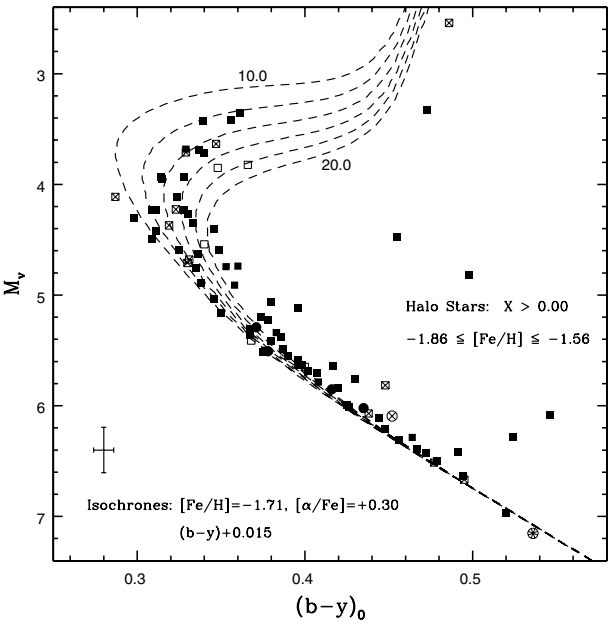

Fig. 10. The $(b–y)_0$, M_V diagram for halo stars ($X > 0.00$) with metallicities of [Fe/H] ≈ −1.71. The symbols are the same, the isochrones from the same sources, and the error bars defined in the same way as for Fig. 8. The stars plotted (minus the binary and variable stars) have a mean value for [Fe/H] of −1.71, exactly the same value as for the isochrones. The isochrones have been shifted by +0.015 in $(b–y)_0$ to provide a better fit for the redder, main-sequence, little-evolved stars.

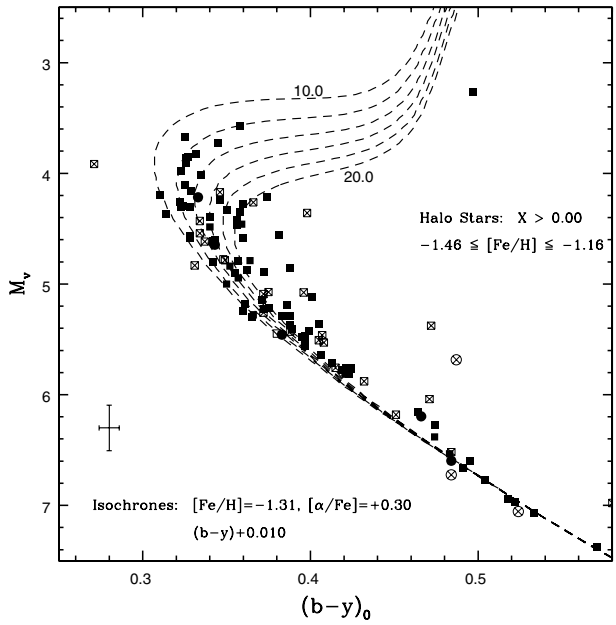

Fig. 11. The $(b–y)_0$, M_V diagram for halo stars ($X > 0.00$) with metallicities of [Fe/H] ≈ −1.31. The symbols are the same, the isochrones from the same sources, and the error bars defined in the same way as for Fig. 8. The stars plotted (minus the binary and variable stars) have a mean value for [Fe/H] of −1.31, exactly the same value as for the isochrones. Here the isochrones have been shifted by +0.010 in $(b–y)_0$ to provide a better fit for the redder, main-sequence, little-evolved stars.

Schuster et al. (1996); only VMP stars classified TO, MS, SG, or BS-TO (the turn-off, main sequence, and subgiant stars) have been plotted. An obvious lower ridge-line is seen, whose $(b–y)_0$ varies with [Fe/H], as one would expect. In the lower panel one can see that this ridge-line corresponds to 13 ± 1 Gyr. The isochrones given are those for [α/Fe] = +0.30, which is appropriate for the more metal-poor stars, [Fe/H] $\lesssim -0.8$ (Márquez 2004; Bressan 2004; Barbuy et al. 2003; Clementini et al. 1999; McWilliam 1997; Nissen & Schuster 1997; Carney 1996; Carney et al. 1997).

A number of stars bluer than this ridge-line are noted, especially over the metallicity range, $-1.5 \lesssim$ [Fe/H] $\lesssim -0.9$, where there are stars with ages reaching ≈ 8 Gyr younger than the ridge-line. These are probably stars analogous to the blue, metal-poor (BMP) stars of Preston et al. (1994) with [Fe/H] < −1.0 and $0\overset{m}{.}15 < (B-V)_0 < 0\overset{m}{.}35$, bluer than the globular cluster turnoffs. At even lower metallicities there are stars with ages ≈3 Gyr younger than the ridge-line, and this is very similar to differences discussed for Figs. 10 and 11 of Paper X, where the VMP stars were compared to the turn-off of the globular cluster M92.

These BMP stars have been discussed in the literature, for example Preston et al. (1994) and Unavane et al. (1996), as being the result of accretion events by the Galaxy of metal-poor, intermediate-age dwarf spheroidal satellites. But they have also been interpreted, for example by Preston & Sneden (2000) and by Carney et al. (2005), as containing a large fraction, "at least half", of blue stragglers.

7.3. Stellar groups in the $(b–y)_0$, M_V diagram

In Figs. 10–12 are shown the $(b–y)_0$, M_V diagrams for three stellar-population, metallicity-range groups. Figures 10 and 11 show "halo" groups ($X > 0.00$) according to the stellar population parameter defined in SPC and shown above in Fig. 5; Fig. 12 presents a "thick-disk" group according to $-21.0 \le X \le -6.0$. This latter thick-disk range assumes that the thick disk is a single stellar population, as shown for example in Figs. 1b and 8b of SPC and in Fig. 3 of this paper, but contradicted by Figs. 6 and 7. The cuts at $X = -21.0$ and $X = -6.0$ serve to reduce the contamination by other stellar populations, such as the halo and old-thin-disk, as shown in Fig. 6 of this paper and Fig. 8b of SPC, while retaining an adequate sample size. This "thick-disk" definition gives 305 stars with a vertical velocity dispersion of $\sigma_{W'} = 52.6$ km s^{-1} from our total sample of 1533 stars, and 246 stars with $\sigma_{W'} = 53.1$ km s^{-1} from the cleaned sample of 1223 stars. As mentioned above, these vertical velocity dispersions are probably larger than the actual true dispersion of the thick disk, due to contamination by the halo, which is obvious in Fig. 6.

In Fig. 10 halo stars with $-1.86 \le$ [Fe/H] ≤ -1.56 are compared to isochrones with [Fe/H] = −1.71; these are the same isochrones as used above in Figs. 8 and 9, those of Bergbusch & VandenBerg (2001; Clem et al. 2004). In Fig. 11 halo stars with $-1.46 \le$ [Fe/H] ≤ -1.16 are compared to isochrones with [Fe/H] = −1.31, and in Fig. 12, thick-disk stars with $-1.03 \le$ [Fe/H] ≤ -0.63 are compared to isochrones with [Fe/H] = −0.83. In all these cases [α/Fe] = +0.30

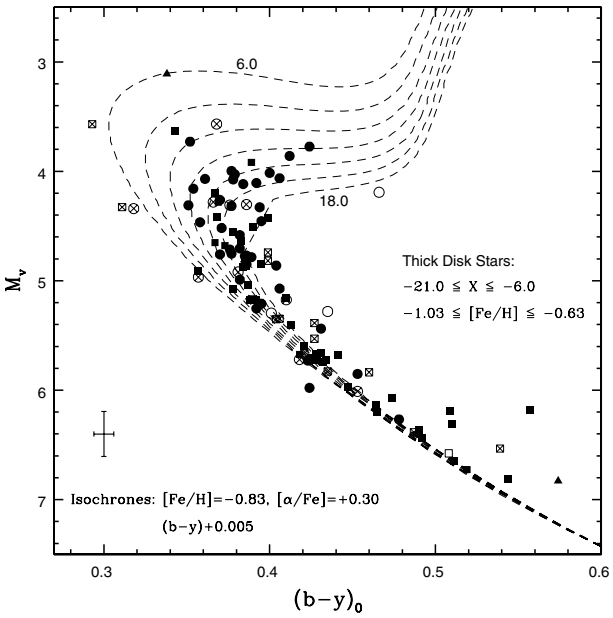

Fig. 12. The $(b–y)_0$, M_V diagram for thick disk stars ($-21.0 \leq X \leq -6.0$) with metallicities of [Fe/H] ≈ -0.83. The symbols are the same, the isochrones from the same sources, and the error bars defined in the same way as for Fig. 8. The stars plotted (minus the binary and variable stars) have a mean value for [Fe/H] of −0.76, slightly larger than that of the isochrones. The isochrones have been shifted by +0.005 in $(b–y)_0$ to provide a better fit for the redder, main-sequence, little-evolved stars.

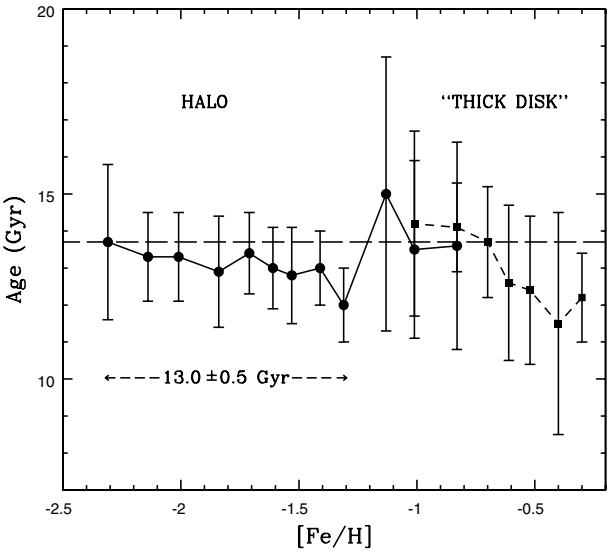

Fig. 13. The [Fe/H], age diagram for halo and "thick disk" stars. The ages have been derived from $(b–y)_0$, M_V diagrams, as in Figs. 10–12. The ages and error bars have been estimated from the 4–10 most evolved stars in each diagram, and the smaller error bars result from those cases where a clear evolving sequence is noted; outliers probably from other stellar populations, as seen in Fig. 12, have been excluded. These error bars represent the estimated error for a single determination (single star), and so should be divided by factors of 2–3 for a mean error. The solid circles and solid line show the results for the halo stars, as defined in the [Fe/H], V(rot) diagram of Fig. 5 ($X \geq 0.0$), and the solid squares and dashed line the results for the "thick disk" stars from the same [Fe/H], V(rot) diagram ($-21.0 \leq X \leq -6.0$). The horizontal dashed line corresponds to 13.7 Gyr from Bennett et al. (2003), the WMAP results for the age of the Universe. The nine most metal-poor "halo" points give an average of 13.0 Gyr with a scatter of ±0.5 Gyr and a mean error of about ±0.2 Gyr.

has been used, which is appropriate, on the average, for stars with [Fe/H] $\lesssim -0.8$ (Márquez 2004; Bressan 2004; Barbuy et al. 2003; Clementini et al. 1999; McWilliam 1997; Nissen & Schuster 1997; Carney 1996; Carney et al. 1997). For metallicities in the range $-0.83 \leq$ [Fe/H] ≤ -0.30, the [α/Fe] values used to determine the ages of the stellar groups have been interpolated between +0.30 and 0.00, as a function of [Fe/H], according to a mean relation for field stars developed by Márquez (2004) using spectroscopic values from several recent sources, as mentioned above. Also noted in Figs. 10–12, the isochrones have all been corrected slightly in $(b–y)_0$ so that the lower theoretical main sequence of the isochrones, $(b–y)_0 \gtrsim +0.40$, matches more closely the lower observed main sequence. These small corrections, $0^m.005$–$0^m.015$ are merely fine adjustments to the very carefully derived color–$T_{\rm eff}$ relations of Clem et al. (2004).

In Fig. 10 a clear sequence of non-binary stars is seen with a mean age of 13.4 ± 1.1 Gyr, from the six most evolved halo stars; in Fig. 11, 12.0 ± 1.0 Gyr, from the eight most evolved, non-binary, halo stars; and in Fig. 12, 14.1 ± 1.2, from the ten most evolved, non-binary, thick-disk stars. In Fig. 12 contamination from another stellar population (the old-thin-disk) is seen with stars as young as 6.0 Gyr, but these have not been included in our average age nor in the statistics. The errors given above are standard deviations for a single determination (single star) within each sequence, assuming that each sequence is in fact isochronic, which may not strictly be the case. These estimated errors are smaller when the evolving sequence is well defined with more evolving stars and little contamination from other stellar populations, and larger when the evolving sequence is not well defined with few evolving stars and more contamination, as seen below in Fig. 13.

8. Age comparisons

8.1. Age versus [Fe/H] diagram

In Fig. 13 the [Fe/H], age diagram is plotted for 12 halo groups ($X \geq 0.0$) over the metallicity range $-2.31 \leq$ [Fe/H] ≤ -0.83, and for 7 "thick disk" groups ($-21.0 \leq X \leq -6.0$) over the metallicity range $-1.01 \leq$ [Fe/H] ≤ -0.30. These metallicity ranges are defined in part by the range for the isochrones of Bergbusch & VandenBerg (2001; Clem et al. 2004) ($-2.31 \leq$ [Fe/H] ≤ -0.30) and in part by the intervals in the stellar population parameter X. For example, in Fig. 5 halo stars ($X \geq 0.0$) can be seen to metallicities as high as [Fe/H] ≈ -0.2, but there are far too few of these for [Fe/H] $\gtrsim -0.8$ to define any sort of age sequence. The same for "thick disk" stars for metallicities less than [Fe/H] ≈ -1.0.

Most of the error bars of Fig. 13 are in the range, $1.0 \lesssim \sigma_{\rm age} \lesssim 2.0$ for a single determination (single star) except where there are too few evolving stars to define a good sequence or where there is contamination by other stellar populations.

For example, at [Fe/H] = −2.31 the halo sample should not be suffering any contamination by disk stars, but there are few (≈4) evolving stars to define a good age sequence, and these show more scatter perhaps due to increasing influence by the detailed chemical abundances, such as [N/Fe] and [C/Fe], upon the *uvby* photometry (see Paper X). Over the range −1.13 ≤ [Fe/H] ≤ −0.83 the halo samples are suffering decreasing numbers of stars, few of which are evolved, and perhaps some small contamination by the thick disk; the error bars are larger, 1–4 Gyr. Over the range −0.61 ≤ [Fe/H] ≤ −0.40 the "thick disk" samples show larger error bars (2–3 Gyr) probably due to several reasons: there are fewer than eight evolving stars for each sample; probable small contaminations by both the old-thin-disk and halo, as seen in Fig. 6, so that the evolving sequences are not well defined; and also the differing ages between the two "thick disk" components discussed above in Sects. 6.3 and 7.1.

In Fig. 13 the halo stars show a slight decrease in mean age over the range −2.31 ≤ [Fe/H] ≤ −1.31 with an average age of 13.0 Gyr and a single-value standard deviation of ±0.5; this reduces to approximately ±0.2 for the mean error of the nine points. The age-metallicity relation which is seen for the halo points in Fig. 13 is not significant considering the single-value error bars, and only marginally significant for the mean-value error bars. Over the range −1.13 ≤ [Fe/H] ≤ −0.83, this age-metallicity relation breaks down completely, and the error bars have grown considerably for the reasons mentioned in the previous paragraph: few evolved stars and perhaps some small contamination by the thick disk.

The horizontal dashed line of Fig. 13 corresponds to 13.7 Gyr from Bennett et al. (2003), the WMAP results for the age of the Universe. The results of Fig. 13 would then suggest that the first stars of the Galaxy formed 0.7 ± 0.3 Gyr after the creation of the Universe, combining our mean error with that of the WMAP value. For this combined mean error, we have assumed that the systematic errors of the isochrones are negligible, based on the continuing high-quality work of Bergbusch & VandenBerg (2001) for stellar models and isochrones, the very carefully derived empirical color–temperature relations of Clem et al. (2004) for *uvby* photometry, and the smallness of the color corrections that we have applied, as seen in Figs. 10–12. Time and continued use of these isochrones and color–temperature relations will test this assumption. Also, the supposition that [α/Fe] = +0.30 for the halo stars may introduce a systematic difference; if in fact [α/Fe] = +0.35 is more realistic for the halo stars over −2.3 ≲ [Fe/H] ≲ −1.3, as suggested in some studies (Márquez 2004), the mean halo age of Fig. 13 would drop by about another 0.3 Gyr.

The "thick-disk" points of Fig. 13 show a very strong age-metallicity correlation, but again this is not highly significant considering the single-value error bars. And, this correlation can mostly be explained as due to varying contributions of the two "thick-disk" components discussed above in Sects. 6.3 and 7.1, one with ([Fe/H], V(rot),X) ≈ (−0.7 dex, +120 km s^{-1}, −9.0) and the other with ([Fe/H], V(rot), X) ≈ (−0.4 dex, +160 km s^{-1}, −21.0). For the points of Fig. 13 the ages have been determined using metallicity intervals of ±0.15 or ±0.20 dex in [Fe/H], the wider range being used to include more stars when needed in the $(b–y)_0$, M_V diagram. So, for the "thick-disk" cut which we are using in Fig. 13, −21.0 ≤ [Fe/H] ≤ −6.0, at [Fe/H] = −1.01, −0.83, and −0.70 the first of the two above "thick-disk" components dominates, and this has the larger age of 11–14 Gyrs, as shown in Fig. 8b and as discussed in Sect. 7.1. At [Fe/H] = −0.40 and −0.30 the second "thick-disk" components dominates, and this has the smaller age of 9–11 Gyrs as shown in Fig. 8a. For metallicities in between there are varying contributions of these two components to the mean ages plotted in Fig. 13.

8.2. Episodes during the Galactic formation and evolution?

The previous figures and discussions point to several evidences for different episodes or physical processes during the formation and evolution of the Galaxy. The most obvious of these, which has been discussed amply in the literature, is the dichotomy seen in Figs. 5 and 7a, between the Galaxy's halo and disk. For example, in Fig. 5 the oval concentration of stars centered at [Fe/H], V(rot) ≈ (−0.25, +180 km s^{-1}) with ranges of approximately ±70 km s^{-1} in V(rot) and approximately ±0.5 dex in [Fe/H], corresponds to the "high-velocity disk" as discussed in Paper V and in SPC. This component of Fig. 5 is made up of mostly disk stars, old-thin and thick, with some small contamination by the halo, as indicated in Fig. 6. The second obvious component of Fig. 5 is that of the halo, more dispersed, centered at [Fe/H], V(rot) ≈ (−1.5, −25 km s^{-1}) with ranges of approximately ±250 km s^{-1} in V(rot) and approximately ±1.35 dex in [Fe/H]. As seen in Fig. 6 and in Fig. 8b of SPC, this stellar component is mostly uncontaminated by the other stellar populations.

But in Figs. 6, 7, and 9 there are other indications of episodes during the Galactic evolution: within the "high-velocity disk" from Figs. 6 and 7, and within the halo from Fig. 9. The sharp drop in the number of stars at X ≈ −15.0, ([Fe/H], V(rot)) ≈ (−0.5−−0.6 dex, 140–150 km s^{-1}), seen in the histogram of Fig. 6, indicates the separation of two events or physical processes at values of metallicity and velocity were the "thick disk" has normally been studied (see SPC). The contours of Fig. 7b show two probable components between the peaks of the old-thin disk and of the halo; these are separated at X ≈ −15.0. The chemodynamic galaxy formation code of Brook et al. (2004) proposes that the thick disk was formed during an epoch of "...multiple mergers of gas-rich building blocks...", that such a scenario fits best the observed kinematic, chemical, and age characteristics of the Galaxy's thick disk. Perhaps what is seen in Figs. 7 and 8 is evidence for two such accretion events, one about 12.5 Gyr ago and another about 10 Gyr.

In Fig. 9, the $(b–y)_0$, [Fe/H] diagram shows evidence for at least two episodes, or intervals, in the evolution of the Galactic halo. Over the metallicity range −1.5 ≲ [Fe/H] ≲ −0.9 there are numerous stars which are younger by as much as 8 Gyr than the ridge-line defined by the large majority of halo stars. For [Fe/H] ≲ −1.5 these younger stars are much less obvious, but there is a number of stars up to 3 Gyr younger than this

ridge-line. Preston et al. (1994) have argued that their blue, metal-poor stars, those with [Fe/H] < -1.0 and $0\overset{m}{.}15 < (B-V)_0 < 0\overset{m}{.}35$, bluer than the globular cluster turnoffs, are evidence for the accretion by the Galaxy of stars from other dwarf galaxies. (Preston & Sneden (2000) and Carney et al. (2005) would argue that many of these BMP stars are in fact blue stragglers.) Also, in Paper X arguments have been made that the younger very metal-poor stars ([Fe/H] $\lesssim -1.5$) present evidence for the hierarchical star-formation/mass-infall of very metal-poor material to the Galaxy and/or for the accretion of material from other (dwarf) galaxies with different formation and chemical-enrichment histories. However, the spectroscopic study of Venn et al. (2004) "...rules out continuous merging of low-mass galaxies similar to these dSph satellites during the formation of the Galaxy". The detailed chemical abundances of the local dwarf galaxies are too different from those of the stellar components of the Galaxy. Only for [Fe/H] ≤ -1.8 might such a scenario work, since for this range the chemistries of the dSphs are in fair agreement with the Galactic halo stars. It would interesting to observe spectroscopically whether the bluer, metal-poor stars of Fig. 9, those with $-1.5 \lesssim$ [Fe/H] $\lesssim -0.9$, have detailed abundances more like the local dSphs or more like the other stellar components of the Galaxy. Also, it would be interesting to observe these BMP stars of Fig. 9 for evidence of binary stars with low-eccentricity orbits, higher-than-average rotational velocities, and lithium deficiencies, all indications for probable blue stragglers (Preston & Sneden 2000; Carney et al. 2005).

In any case Fig. 9 indicates some sort of main formation event for the Galaxy 13–14 Gyr ago, such as a collapse, as shown by the ridge-line, and then formation of the more metal-poor stars, [Fe/H] $\lesssim -1.5$, for as long as 3 Gyr afterwards, and, perhaps, of less metal-poor stars, $-1.5 \lesssim$ [Fe/H] $\lesssim -0.9$, for as long as 8 Gyr afterwards.

8.3. Galactic and cosmological implications

8.3.1. The thick disk

As mentioned above and as seen in Figs. 6–8, evidence for two episodes (or Galactic components) between the old thin disk and halo can be detected in our data base of high-velocity and metal-poor stars. These stellar thick-disk components have ([Fe/H], V(rot), X, Age, $\sigma_{W'}$) $\approx$ (-0.7 dex, 120 km s^{-1}, -9.0, 12.5 Gyr, 62.0 km s^{-1}) and $\approx$ (-0.4 dex, 160 km s^{-1}, -21.0, 10.0 Gyr, 45.8 km s^{-1}), with some contamination to these values by the other stellar populations, especially the halo to the former group as can be seen in Fig. 6. Parker et al. (2003, 2004) and Gilmore et al. (2002) also find evidence for two components within the thick disk. Parker et al. use both star-count and kinematic evidence to argue for the existence of an "asymmetric thick disk" with significant differences between the quadrants I and IV of the Galaxy. Quadrant I has a significant (20–25%) excess of stars over the counts in quadrant IV, and a rotation lag of 80–90 km s^{-1} compared to a lag of only 20 km s^{-1} for quadrant IV. They mention three possibilities to explain this "asymmetric thick disk": the fossil remnant of a galaxy merger, a triaxial thick disk, or an interaction between the thick disk and the Galactic bar; they prefer the latter explanation but hedge their final conclusions mentioning the recently discovered debris stream in Canis Major (Martin et al. 2004). Velázquez & White (1999) have proposed the formation of asymmetric disks as the result of galactic accretion processes.

Gilmore et al. (2002) also find evidence for two probable components within the thick disk by studying stars 0.5–5.0 kpc from the Galactic plane. Surprisingly they find a V(rot) a few kpc above the plane of only about 100 km s^{-1} compared to the expected 180 km s^{-1}, i.e. an excess lag of about 80 km s^{-1}, and conclude that this is probably evidence for a merger event with the disk of the Milky Way some 10–12 Gyr ago, that their sample is dominated by the remnants of a disrupted satellite galaxy. These values for the rotational lag and age agree quite well with our values given above for the first thick-disk component mentioned above. According to the arguments of Gilmore et al., our component with [Fe/H] ≈ -0.70 would represent the remnants of a shredded satellite from an early merger, while the component with [Fe/H] ≈ -0.40 the more "classical" thick disk or perhaps a later merger that provided the main mass of the local thick disk.

The discovery of the probable satellite remnant in Canis Major by Martin et al. (2004; also Bellazzini et al. 2004; Martin et al. 2005; Bellazzini et al. 2005; Dinescu et al. 2005) provides very serious observational confirmation and explanation for the above results of Gilmore et al. and perhaps also those of Parker et al.[4]. This debris stream orbits very close to the Galactic plane, with a pericenter close to the solar distance, $R_\odot$, and with an orbital eccentricity and vertical scale height similar to that of the thick disk. Martin et al. conclude that the Galactic thick disk is continually growing, even up to the present epoch, and that dwarf galaxies on nearly co-planar orbits, such as the precursor of the Canis Majoris remnant, form the main building blocks of the Galaxy's thick disk. Also, Yoachim & Dalcanton (2005) have observed counterrotating thick disks in external galaxies and claim that this too strongly supports the idea that thick disks form from the direct accretion of infalling satellite galaxies. Yong et al. (2005) discuss the unusual elemental abundance ratios of the open clusters in the outer Galactic disk, and propose that the formation of these outer clusters may have been triggered by a series of merger events in the outer disk, such as the Canis Majoris event. These results point to the conclusion that one, or perhaps both, of the thick-disk components documented above in our Figs 6–8 are due to satellite remnants, debris streams, such as that observed in Canis Major. The disrupting dwarf galaxy discovered in Sagittarius by Ibata et al. (1994) also provides such possibilities for structure within the Galaxy's halo and thick disk.

The Galactic models given and documented by Kroupa (2002), Abadi et al. (2003), and Brook et al. (2004) also provide

[4] The reality of the Canis Majoris dwarf galaxy is still in doubt; Momany et al. (2004) propose that Martin et al. are really looking at the southern Galactic warp, and Carraro et al. (2005) argue that this Canis Majoris "dwarf galaxy" and its Blue Plume are really substructures in the Norma-Cygnus and Perseus spiral arms and their inter-arm region.

support for probable structure within the thick disk, such as that described above. The work of Kroupa predicts the thickening of the Galactic disk through "clustered star formation" induced by the interaction of the Galactic disk with passing satellite galaxies. He proposes that star clusters are the "building blocks" of the Galaxy, that massive clusters add kinematically hot components to the Galactic field stellar populations, and that for ages >3 Gyr ago the Galaxy suffered a period with an ICMF (initial cluster mass function) extending to very massive clusters. This scenario is very useful in light of the chemical-difference results of Venn et al. (2004) comparing the detailed abundances of the local dwarf galaxies with those of the thick disk in that direct infall of the passing satellite is not needed to heat the disk. Under such a scheme, the two thick-disk components seen in Fig. 7 might have been caused by two major interactions of the Galactic disk with passing satellite galaxies.

The models of Abadi et al. and Brook et al. both make use of hierarchical clustering (merging) within a ΛCDM universe and obtain similar results. They do not specifically model the Milky Way but a very similar late-type galaxy, and produce results very interesting for explaining the thick disk and also the behavior shown in our Figs. 6–8. The model of Abadi et al. produces starbursts (their figure 7) triggered by merger and accretion events with major episodes occurring at 8.5, 10.0, 11.5, and 13.0 Gyr ago. They predict that about 15% of the thin disk and more than 60% of the thick disk are made up of tidal debris from satellite galaxies; for ages older than ≈10 Gyr, about 90% of the thick disk shares this origin. For this model the tidal disruption of satellite galaxies is seen as the main process of assembly of their simulated thick disk, within distinct episodes. The "chemodynamical" galaxy formation code of Brook et al. produces the thick disk at ages greater than ≈8 Gyr during a very chaotic period during the end of the peak SFR. The thick-disk stars are formed from "gas-rich building blocks" accreted to the galaxy during such a period that is the "natural consequence" of the early, violent hierarchical clustering of the ΛCDM universe. They predict that thick disks should be prevalent for disk galaxies. The structure seen in our Figs. 6–8 would suggest two rather significant "gas-rich building blocks" or accretion episodes for the Milky Way thick disk.

However, it is more difficult to accommodate these latter two models to the results of Venn et al. (2004), who compared the detailed chemical signatures of the Galactic stellar populations with those of the local dwarf galaxies. They conclude that the thick disk is not comprised of remnants of low-mass dSph galaxies nor of remnants of higher-mass dwarf galaxies such as the LMC or the one in Sagittarius, "because of differences in chemistry." However, the accretion of gas-rich components, such as in the model of Brook et al., rather than actual stars, may circumvent this discrepancy.

8.3.2. The bluer, metal-poor stars

In our Fig. 9 a very distinct difference is seen between the blue limits over the range $-1.5 \lesssim$ [Fe/H] $\lesssim -0.9$ as compared to the blue limits over [Fe/H] $\lesssim -1.5$. The majority of halo stars ($X >$ 0.0) and very-metal-poor stars form a ridge-line corresponding to 13–14 Gyr, while for the former [Fe/H] interval the bluest stars are ≈8 Gyr younger but only about 2–3 Gyr younger over the latter interval (see also Figs. 10–11 of Paper X). These stars are very analogous to the BMP stars of Preston et al. (1994), which have [Fe/H] $\lesssim -1.0$ and fall blueward of the most metal-poor globular cluster turnoffs, $0.15 \lesssim (B-V)_0 \lesssim 0.35$. Preston et al. find an isotropic velocity dispersion for the BMPs, $\sigma_{r\phi\theta} \approx$ 90 km s^{-1} and conclude that these BMP stars probably were accreted to the Galaxy from dwarf spheroidal satellites during the last ≈10 Gyr. But why the dichotomy at [Fe/H] ≈ −1.5?

Figure 2 of Unavane et al. (1996), $(B-V)_0$ versus [Fe/H], is very similar to our Fig. 9. Their figure does not distinguish between halo and thick-disk stars but plots "metal-poor" stars from the proper-motion-selected sample of Carney et al. (1994). Again, a ridge-line is seen corresponding to an age of 15–16 Gyr (according to the revised Yale Isochrones) with bluer stars extending ≈8 Gyr to younger ages over the interval $-1.5 \lesssim$ [Fe/H] $\lesssim -1.0$ and only 2–3 Gyr younger for [Fe/H] $\lesssim -1.5$, very analogous to our Fig. 9, except for a 2 Gyr offset in the absolute ages. They estimate that this younger-star population makes up about 5% of the stars in the most metal-poor range, [Fe/H] < -1.95, about 8% in the intermediate range, $-1.95 <$ [Fe/H] < -1.5, but about 34% over the range $-1.5 <$ [Fe/H] < -1.0. They also compare these bluer stars to the turnoff colors seen in local dSph galaxies and try to estimate the possible number of mergers by Carina-like galaxies (≈60) or by Fornax-like dwarfs (≈6) to produce these BMP stars.

Seen in terms of a hierarchical-clustering scheme and, for example, Fig. 7 of Abadi et al. 2003, Fig. 9 shows that the initial clustering was rather abrupt, as shown by the ridge-line, tapering off rather quickly for 2–3 Gyr afterwards. Then later there was an episode (or episodes) such as the accretion of a dwarf galaxy (galaxies) that brought in material with [Fe/H] ≈ -1.2 ± 0.3 dex, forming or bringing stars as much as 8 Gyr younger than the typical halo star. One might conclude that the youngest of these stars formed during the accretion event ("starburst") itself, about 5–6 Gyr ago. It would interesting to study the detailed chemical abundances of the BMP stars seen in Fig. 9, those with $(b-y) \lesssim 0.30$ and $-1.5 \lesssim$ [Fe/H] $\lesssim -0.9$: BD+25°1981, BD−12°2669, G202–065, BPS BS 15621–0070, BPS BS 16026–0073, BPS BS 16081–0038, BPS BS 17444–0059, BPS BS 17581–0075, BPS BS 17581–0077, BPS CS 22887–0048, BPS CS 30311–0068, and BPS CS 30493–0001, and interpret these in the light of the conclusions made by Venn et al. (2004). Do these stars have chemical abundances more like those of the Galactic stellar populations, or more like those of the local dwarf galaxies? Was the formation of these stars induced by the close passage of a satellite galaxy (the clustered star formation of Kroupa 2002), or were they actually brought into the Galaxy by the merger/accretion of the satellite (Abadi et al. 2003)? Alternatively, do they show the characteristics of blue stragglers? The first three stars listed above (BD+25°1981, BD−12°2669, G202–065) have been studied as probable metal-poor field blue stragglers by Carney et al. 2005. (The coordinates and characteristics of the above BPS stars are given in the tables of Paper X, also available at the CDS).

8.3.3. The oldest stars

Figure 13, a plot of mean stellar ages versus [Fe/H], derived from $(b–y)_0$, M_V diagrams such as those in Figs. 10–12, shows that in general our ages are in agreement with the WMAP results for the age of the Universe (Bennett et al. 2003), 13.7 ± 0.2 Gyr. The halo groupings agree very well, with an average 13.0 ± 0.2 Gyr (mean error). Over the range $-1.2 \lesssim$ [Fe/H] $\lesssim -0.8$ some of our ages are larger than the WMAP result, but this is the interval where the stellar populations (especially the halo and thick disk) are most mixed and difficult to separate, where the BMP-star contribution to the halo groupings is most important (Sect. 8.3.2), where the stellar sequences in the $(b–y)_0$, M_V diagrams are least well defined, and where the estimated errors of the groupings are the largest, ±2–4 Gyr. None of the largest ages in Fig. 13 are discrepant with the WMAP result at the 2σ level (mean errors); in fact, the most incongruent is only about 1σ greater than the WMAP age.

From the nine most metal-poor halo groupings of Fig. 13, we estimate a time interval of 0.7 ± 0.3 Gyr from the beginning of the Universe to the formation of the Galactic halo. This compares quite favorably with the estimate of 0.8–1.0 Gyr that Krause (2003, 2004) and Krauss & Chaboyer (2003) estimate using globular cluster ages. The WMAP results (Bennett et al. 2003) also indicate that reionization occurred at an age of 0.1–0.4 Gyr (180^{+220}_{-80} Myr), leaving 0.6–0.3 Gyr for the formation of the Galactic Population II, which is entirely feasible considering that there is considerable agreement that the zero-metallicity/very-low-metallicity Population III had a high-mass heavy IMF (Bromm et al. 1999, 2002; Abel et al. 2000; Nakamura & Umemura 2001; Hernandez & Ferrara 2001; Bromm 2004; Omukai et al. 2005); these studies all point to the first generation stars having mostly stars in the range 10–100 $M_\odot$, or even higher. The zero-metallicity stellar models of Marigo et al. (2001) indicate that such massive, metal-free stars, in the range 10–100 $M_\odot$, have nuclear lifetimes of 3×10^6 to 2×10^7 yrs. So, there is more than enough time for the zero-metallicity/very-low-metallicity Pop. III stars to evolve, enrich the interstellar medium, and set the stage for the Pop. II, more-metal-rich stars to follow. These results also corroborate Krause (2003) and provide another "hint" for a time interval between reionization and the formation of larger-scale structures, such as the Galactic halo and globular clusters.

Also seen in Fig. 13 are mean ages for thick disk stars, those selected using the criterion $-21.0 \leq X \leq -6.0$ from the [Fe/H], V(rot) diagram. Some of these thick-disk groups are seen to be as old as the halo stars, which agrees with the hierarchical clustering models of Abadi et al. (2003) and Brook et al. (2004). For example in the case of Abadi et al., the stars in the outermost, presumably most metal-poor regions of the accreting satellites contribute primarily to the Galaxy's halo and thick disk, since they can be more easily stripped, while those in the core are more resistant to disruption, have more time to have their orbits circularized by dynamical friction, and so end up in the old thin disk. About 50% of the spheroid and 60% or more of the thick disk share their origin in the same merger/accretion events; for the older thick disk (ages $\gtrsim$ 10 Gyr) about 90% of the stars were brought to the galaxy in this way. So, many of the halo and thick-disk stars participated in the same merger/accretion events and should have similar ages.

The thick-disk component of Fig. 13 also shows a very clear age-metallicity relation with the more metal-poor thick-disk stars ([Fe/H] ≈ -1.0) being ≈3 Gyr older than the higher-metallicity ones ([Fe/H] ≈ -0.3). This agrees, at least qualitatively, with the age-metallicity relation found for the Galactic thick disk by Bensby et al. (2004). Their Figs. 5 and 8 show a somewhat larger range in ages, 4–5 Gyr, but they are also working over a somewhat greater range in [Fe/H], −0.90 to 0.00. Their largest ages for the thick disk, 12–15 Gyr, agree well with our largest as seen in Fig. 13, but their smaller ages, 6–10 Gyr, are less than ours, due mostly to the fact that they are able to track the thick disk to [Fe/H] = 0.0, while we work only to the limit of the available isochrones, [Fe/H] = −0.30. At [Fe/H] = −0.30 Bensby et al. (2004) obtain ages of 8–11.5 Gyr for the thick disk, slightly lower than in our Fig. 13. Also, their method for separating out the thick-disk stars is more rigorous, and strictly kinematic, making use of the velocity dispersions and asymmetric drifts for the three stellar populations (thin disk, thick disk, and halo), while our method uses only the X criterion, a function of [Fe/H] and V(rot) as described above. And, much of our age-metallicity relation is produced by the different mean characteristics of the two thick-disk components discussed above in Sect. 8.3.1; one has (age,[Fe/H])≈(12.5 Gyr, −0.7 dex) and the other ≈(10.0, −0.4). In any case, we would agree mostly with at least two of the main conclusions of Bensby et al.: that the star formation of the thick disk was ongoing for several Gyr, and that the thick disk was the result of merger and/or interaction events with satellite galaxies. The Fig. 7 of Abadi et al. 2003 shows the thick-disk phase of the galaxy formation ongoing for 5–6 Gyr.

In many of the $(b–y)_0$, M_V diagrams, such as Figs. 8, 10, 11, and 12, stars are plotted which appear to have ages greater than 14–16 Gyr, sometimes much greater. The mean ages plotted in Fig. 13 generally represent well-formed sequences at the younger extreme of these $(b–y)_0$, M_V diagrams, but frequently "older" stars are present. For example, in Fig. 11 a sequence of eight stars is seen which follows the 20-Gyr isochrone, as well as a number of stars which appear even older, and not all of these have been identified as binaries. If these stars really are this old would impose serious cosmological implications! But a number of other possibilities have to be considered: (a) unidentified binaries; certainly not all binaries have been recognized through photometric and radial-velocity studies; (b) larger than mean observational errors; the error bars which are shown represent $\pm 1\sigma$ error, and approximately 5% of the stars will have errors in M_V and $(b–y)_0$ larger than 2σ; (c) unusual chemical compositions and their effects upon the photometric indices; as discussed in Paper X, the c_0 index may be shifted by anomalous carbon and nitrogen abundances via the NH, CH, and CN molecular bands, and these effects will increase with decreasing temperature. These possibilities suggest a number of future studies, such as detailed, careful, and extended spectroscopic studies of the radial velocities and detailed abundances of those stars which appear older than ≈14–16 Gyr. To confirm

or deny these large ages would have important cosmological connotations.

9. Conclusions

1. The catalogue of *uvby–β* values presented in Table 1 for 442 high-velocity and metal-poor stars is closely on the same photometric systems as the previous catalogues of SN and SPC (see Figs. 1 and 2).
2. The photometric [Fe/H] histogram for our total sample of 1223 high-velocity and metal-poor stars can be fit very well using only three Gaussian components with ($\langle$[Fe/H]$\rangle$, $\sigma_{[Fe/H]}$) = (−1.40,0.60) for the halo Gaussian, (−0.55, 0.18) for the thick disk, and (−0.16, 0.14) for the old thin disk (see Fig. 3).
3. Our empirical, photometric calibration for M_V based on 512 Hipparcos stars with parallax errors less than 10% and cleaned of binaries, has a scatter of $\pm 0\overset{m}{.}206$ and shows no significant systematic problems over the metallicity range $-2.39 \leq$ [Fe/H] ≤ 0.00, as shown in Fig. 4.
4. Our X histogram is not fit well by a three-component Gaussian as previously in SPC, where X is our stellar population parameter, a linear combination of [Fe/H] and V(rot). A sharp drop in the number of stars at $X = -15.0$ falls near the values of ([Fe/H], V(rot), X) where the thick disk had previously been studied in SPC, and may show evidence for structure within the thick disk. (See Fig. 6). A contour plot of the [Fe/H], V(rot) diagram shows two probable components between the old-thin disk and the halo, one with ([Fe/H], V(rot), X, Age, $\sigma_{W'}$) ≈ (−0.7 dex, 120 km s^{-1}, −9.0, 12.5 Gyr, 62.0 km s^{-1}), and the other with ≈ (−0.4, 160, −20.0, 10.0, 45.8). (See Figs. 7 and 8.) This agrees well with the results of Gilmore et al. (2002) and with Parker et al. (2003; 2004) concerning components within the thick disk.
5. The [Fe/H], $(b–y)_0$ diagram for halo stars (Fig. 9) shows different bluest limits between the metallicity ranges, $-1.5 \lesssim$ [Fe/H] $\lesssim -0.9$ and [Fe/H] $\lesssim -1.5$. In the former interval the bluest stars extend to about 8 Gyr younger than the ridge-line defined by most of the halo stars, while in the second interval there are halo stars only about 2–3 Gyr younger than this ridge-line. One could conclude that the initial hierarchical clustering was rather abrupt, tapering off rather quickly for 2–3 Gyr afterwards, and then about 5–6 Gyrs ago an accretion/merger event brought in material with [Fe/H] ≈ −1.2 ± 0.3 dex. (The bluer stars of this metallicity interval have also been interpreted as field blue stragglers.)
6. The present results show considerable evidence for episodes during the formation and evolution of the Galaxy and its stellar populations. The [Fe/H], V(rot) diagram of Fig. 5 shows the very well-known dichotomy between the disk and halo, with the halo having an age of about 13 Gyr (Fig. 13). Figures 6–8 show probable structure within the thick disk, with two components present having ages of about 10 and 12.5 Gyr. The [Fe/H], $(b–y)_0$ diagram of Fig. 9 presents evidence for significant differences as a function of [Fe/H] for the formation of the youngest halo stars, with a probable event having occurred ≈5.5 Gyr ago. All this supports the ΛCDM hierarchical-clustering scheme, such as the model of Abadi et al. (2003), which produces starbursts triggered by merger/accretion events at 8.5, 10.0, 11.5, and 13.0 Gyr for a galaxy model similar to the Milky Way.
7. Our [Fe/H], age diagram (see Fig. 13) indicates that the more metal-poor stars analyzed here, over the range $-2.31 \lesssim$ [Fe/H] $\lesssim -1.31$, have a mean age of 13.0 Gyr, only 0.7 ± 0.3 Gyr younger than the age of the Universe given by the WMAP results of Bennett et al. (2003). This result agrees well with those of Krause (2003, 2004) that the oldest globular clusters formed at about 0.8–1.0 Gyr, and that larger-scale structures, such as the Galactic halo and globular clusters, formed after reionization. An interval of 0.7 ± 0.3 Gyr is sufficient for the formation and complete evolution of zero-metallicity/very-low-metallicity Population III stars, thought to have had a very high-mass heavy IMF.

Acknowledgements. W.J.S. is very grateful to the DGAPA–PAPIIT (UNAM) (projects Nos. IN101495 and IN111500) and to CONACyT (México) (projects Nos. 1219–E9203 and 27884E) for funding which permitted travel and also the maintenance and upgrading of the *uvby–β* photometer. A.M. acknowledges financial support from FCT (Portugal) through grants BPD/20193/99 and SFRH/BPD/19105/2005; and CONACyT (Mexico; project I33940-E). W.J.S. also thanks José Guichard, who extended the invitation to spend a sabbatical year at INAOE, where much of the analysis for this publication has been done, I. Aretxaga, M. Plionis, E. Gaztañaga, ... for an interesting and useful cosmology discussion group, and M. Reyes Muños, G. Hernandez Palacios, and A. López of the computing center of INAOE for much needed help. Don VandenBerg and James Clem made their *uvby* isochrones available prior to publication, and we greatly appreciate it. Bruce W. Carney provided A. Márquez and W. J. Schuster with information concerning the binary-star contamination of their samples prior to publication, and we sincerely thank him. We thank Xavier Hernandez, who helped with useful ideas, discussions, and references. Many people at the SPM observatory have helped over the years; we thank especially L. Gutíerrez, V. García (deceased), B. Hernández, J.L. Ochoa, J.M. Murillo, F. Quiros, E. Colorado, F. Murillo, J. Valdez, B. García, B. Martínez, E. López, A. Cordova, M.E. Jiménez, and G. Puig. This publication has made use of the SIMBAD database, operated at CDS, Strasbourg, France. We would also like to thank Bruce Carney, the referee, for many ideas and references used to polish the final manuscript.

References

Abadi, M. G., Navarro, J. F., Steinmetz, M., & Eke, V. R. 2003, ApJ, 597, 21
Abel, T., Bryan, G. L., & Norman, M. L. 2000, ApJ, 540, 39
Abt, H. A., & Biggs, E. S. 1972, Bibliography of Stellar Radial Velocities, Microfiche version. Centre de Données Stellaires, Observatoire de Strasbourg
Alonso, A., Arribas, S., & Martínez-Roger, C. 1996, A&A, 313, 873
Alonso, A., Arribas, S., & Martínez-Roger, C. 1999, A&AS, 140, 261
Barbier-Brossat, M., Petit, M., & Figon, P. 1994, A&AS, 108, 603
Barbier-Brossat, M., & Figon, P. 2000, A&AS, 142, 217
Barbuy, B., Perrin, M.-N., Katz, D., et al. 2003, A&A, 404, 661
Bellazzini, M., Ibata, R., Monaco, L., et al. 2004, MNRAS, 354, 1263
Bellazzini, M., Ibata, R., Martin, N., et al. 2005 [arXiv:astro-ph/0504494]

Bennett, C. L., Halpern, M., Hinshaw, G., et al. 2003, ApJS, 148, 1
Bensby, T., Feltzing, S., & Lundström, I. 2003, A&A, 410, 527
Bensby, T., Feltzing, S., & Lundström, I. 2004, A&A, 421, 969
Bensby, T., Feltzing, S., Lundström, I., & Ilyin, I. 2005, A&A, 433, 185
Bergbusch, P. A., & VandenBerg, D. A. 2001, ApJ, 556, 322
Bressan, A. 2004, private communication
Brewer, M.-M., & Carney, B. W. 2004, PASA, 21, 134
Bromm, V. 2004, PASP, 116, 103
Bromm, V., Coppi, P. S., & Larson, R. B. 1999, ApJ, 527, L5
Bromm, V., Coppi, P. S., & Larson, R. B. 2002, ApJ, 564, 23
Brook, C. B., Kawata, D., Gibson, B. K., & Freeman, K. C. 2004, ApJ, 612, 894
Carney, B. W. 1996, PASP, 108, 900
Carney, B. W. 2003, private communication
Carney, B. W., Latham, D. W., Laird, J. B., & Aguilar, L. A. 1994, AJ, 107, 2240
Carney, B. W., Wright, J. S., Sneden, C., et al. 1997, AJ, 114, 363
Carney, B. W., Latham, D. W., & Laird, J. B. 2005, AJ, 129, 466
Carraro, G., Vázquez, R. A., Moitinho, A., & Baume, G. 2005, ApJ, 630, L153
Clem, J. L., VandenBerg, D. A., Grundahl, F., & Bell, R. A. 2004, AJ, 127, 1227
Clementini, G., Gratton, R. G., Carretta, E., & Sneden, C. 1999, MNRAS, 302, 22
Crane, J. D., Majewski, S. R., Rocha-Pinto, H. J., & Frinchaboy, P. M. 2003, ApJ, 594, L119
Crawford, D. L. 1975, PASP, 87, 481
Crawford, D. L., & Barnes, J. V. 1970, AJ, 75, 978
Crawford, D. L., & Mander, J. 1966, AJ, 71, 114
Dinescu, D. I., Martínez-Delgado, D., Girard, T. M., et al. 2005, ApJ, 631, L49
Dommanget, J., & Nys, O. 1994, Comm. Obs. Roy. Belgique, Ser. A, 115, 1
ESA 1997, The Hipparcos and Tycho Catalogues, ESA SP–1200 (Noordwijk, Netherlands: ESA Publications Division)
Feltzing, S., Holmberg, J., & Hurley, J. R. 2001, A&A, 377, 911
Feltzing, S., Bensby, T., & Lundström, I. 2003, A&A, 397, L1
Fouts, G., & Sandage, A. 1986, AJ, 91, 1189
Freeman, K. C. 1991, in Dynamics of Disk Galaxies, ed. B. Sundelius (Göteborg: Göteborgs Univ.), 15
Fukugita, M., & Peebles, P. J. E. 2004, ApJ, 616, 643
Furhmann, K. 1998, A&A, 338, 161
Giclas, H. L., Slaughter, C. D., & Burnham, R., Jr. 1959, Lowell Obs. Bull., 4, 136
Giclas, H. L., Burnham, R., Jr., & Thomas, N. G. 1961, Lowell Obs. Bull., 5, 61
Giclas, H. L., Burnham, R., Jr., & Thomas, N. G. 1975, Lowell Obs. Bull., 8, 9
Gilmore, G. 1984, MNRAS, 207, 223
Gilmore, G., Wyse, R. F. G., & Norris, J. E. 2002, ApJ, 574, L39
Grønbech, B., Olsen, E. H., & Strömgren, B. 1976, A&AS, 26, 155
Hernandez, X., & Ferrara, A. 2001, MNRAS, 324, 484
Høg, E., Fabricius, C., Makarov, V. V., et al. 2000, A&A, 355, L27 (the Tycho-2 Catalogue)
Ibata, R. A., Gilmore, G., & Irwing, M. J. 1994, Nature, 370, 194
Ibata, R., Lewis, G. F., Irwin, M., Totten, E., & Quinn, T. 2001, ApJ, 551, 294
Ibata, R. A., Irwin, M. J., Lewis, G. F., Ferguson, A. M. N., & Tanvir, N. 2003, MNRAS, 340, L21
Johnson, H. L., Iriarte, B., Mitchell, R. I., & Wisniewski, W. Z. 1966, Comm. Lunar and Planetary Lab., 4, 99 (Tucson: Univ. of Arizona)
Johnson, R. H., & Soderblom, D. R. 1987, AJ, 93, 864
Karaali, S., Bilir, S., & Hamzaoğlu, E. 2004, MNRAS, 355, 307
Karataş, Y., Bilir, S., & Schuster, W. J. 2005, MNRAS, 360, 1345
Kerber, L. O., Javiel, S. C., & Santiago, B. X. 2001, A&A, 365, 424
Kerr, F. J., & Lynden-Bell, D. 1986, MNRAS, 221, 1023
Krause, L. M. 2003, ApJ, 596, L1
Krause, L. M. 2004, ApJ, 604, 481
Krause, L. M., & Chaboyer, B. 2003, Science, 299, 69
Kroupa, P. 2002, MNRAS, 330, 707
Larsen, J. A., & Humphreys, R. M. 2003, AJ, 125, 1958
Lutz, T. E., & Kelker, D. H. 1973, PASP, 85, 573
Luyten, W. J. 1957, A Catalogue of 9867 Stars in the Southern Hemisphere with Proper Motions Exceeding 0.″20 Annually (Minneapolis: The Lund Press)
Luyten, W. J. 1961, A Catalogue of 7127 Stars in the Northern Hemisphere with Proper Motions Exceeding 0.″20 Annually (Minneapolis: The Lund Press)
Luyten, W. J. 1979a, NLTT Catalogue (Minneapolis: University of Minnesota)
Luyten, W. J. 1979b, LHS Catalogue (Minneapolis: University of Minnesota)
Majewski, S. R., Ostheimer, J. C., Rocha-Pinto, H. J., et al. 2004, ApJ, 615, 738
Marigo, P., Girardi, L., Chiosi, C., & Wood, P. R. 2001, A&A, 371, 152
Márquez, A. 2004, doctoral dissertation, in process
Márquez, A., & Schuster, W. J. 1994, A&AS, 108, 341 (MS)
Martell, S. L., & Laughlin, G. 2002, ApJ, 577, L45
Martell, S. L., & Smith, G. H. 2004, PASP, 116, 920
Martin, N. F., Ibata, R. A., Bellazzini, M., et al. 2004, MNRAS, 348, 12
Martin, N. F., Ibata, R. A., Conn, B. C., et al. 2005 [arXiv:astro-ph/0503705]
McWilliam, A. 1997, ARA&A, 35, 503
Mihalas, D., & Binney, J. 1981, Galactic Astronomy (New York: W. H. Freeman)
Momany, Y., Zaggia, S. R., Bonifacio, P., et al. 2004, A&A, 421, L29
Nakamura, F., & Umemura, M. 2001, ApJ, 548, 19
Newberg, H. J., Yanny, B., Rockosi, C., et al. 2002, ApJ, 569, 245
Nissen, P. E. 1994, in Stars, Gas and Dust in the Galaxy, Invited Reviews at a Symposium in Honor of Eugenio E. Mendoza, ed. A. Arellano Ferro & M. Rosado, Rev. Mex. Astr. Astrofís., 29, 129
Nissen, P. E., & Schuster, W. J. 1991, A&A, 251, 457 (Paper V)
Nissen, P. E., & Schuster, W. J. 1997, A&A, 326, 751
Nordström, B. 2000, private communication
Norris, J. E., & Ryan, S. G. 1989, ApJ, 340, 739
Olsen, E. H. 1983, A&AS, 54, 55
Olsen, E. H. 1984, A&AS, 57, 443
Omukai, K., Tsuribe, T., Schneider, R., & Ferrara, A. 2005, ApJ, 626, 627
Parker, J. E., Humphreys, R. M., & Larsen, J. A. 2003, AJ, 126, 1346
Parker, J. E., Humphreys, R. M., & Beers, T. C. 2004, AJ, 127, 1567
Parrao, L., Schuster, W. J., & Arellano Ferro, A. 1988, Reporte Técnico # 52, Instituto de Astronomía, Universidad Nacional Autónoma de México
Preston, G. W., Beers, T. C., & Shectman, S. A. 1994, AJ, 108, 538
Preston, G. W., & Sneden, C. 2000, AJ, 120, 1014
Prochaska, J. X., Naumov, S. O., Carney, B. W., McWilliam, A., & Wolfe, A. M. 2000, AJ, 120, 2513
Ramírez, I., & Meléndez, J. 2005a, ApJ, 626, 446
Ramírez, I., & Meléndez, J. 2005b, ApJ, 626, 465

Reddy, B. E., Tomkin, J., Lambert, D. L., & Allende Prieto, C. 2003, MNRAS, 340, 304
Reid, N., & Majewski, S. R. 1993, ApJ, 409, 635
Robin, A., & Crézé, M. 1986, A&A, 157, 71
Rocha-Pinto, H. J., Majewski, S. R., Skrutskie, M. F., & Crane, J. D. 2003, ApJ, 594, L115
Rocha-Pinto, H. J., Majewski, S. R., Skrutskie, M. F., Crane, J. D., & Patterson, R. J. 2004, ApJ, 615, 732
Röser, S., & Bastian, U. 1991, PPM Star Catalogue by the Astronomisches Rechen-Institut Heidelberg (Heidelberg: Spektrum Akademischer Verlag)
Ryan, S. G. 1989, AJ, 98, 1693
Ryan, S. G., & Norris, J. E. 1991, AJ, 101, 1835
Salim, S., & Gould, A. 2003, ApJ, 582, 1011
Sandage, A. 1987, AJ, 93, 610
Sandage, A., & Fouts, G. 1987, AJ, 93, 74
Schlegel, D. J., Finkbeiner, D. P., & Davis, M. 1998, ApJ, 500, 525
Schneider, D. P., Fan, X., Hall, P. B., et al. 2003, AJ, 126, 2579
Schuster, W. J., & Nissen, P. E. 1988, A&AS, 73, 225 (SN)
Schuster, W. J., & Nissen, P. E. 1989a, A&A, 221, 65 (Paper II)
Schuster, W. J., & Nissen, P. E. 1989b, A&A, 222, 69 (Paper III)
Schuster, W. J., & Parrao, L. 2001, Rev. Mex. Astr. Astrofís., 37, 187
Schuster, W. J., Parrao, L., & Contreras Martínez, M. E. 1993, A&AS, 97, 951 (SPC)
Schuster, W. J., Nissen, P. E., Parrao, L., Beers, T. C., & Overgaard, L. P. 1996, A&AS, 117, 317
Schuster, W. J., Parrao, L., & Guichard, J. 2002, The Journal of Astronomical Data, 8, No. 2, 1
Schuster, W. J., Beers, T. C., Michel, R., Nissen, P. E., & García, G. 2004, A&A, 422, 527 (Paper X)
Strömgren, B. 1966, ARA&A, 4, 433
Thorburn, J. A. 1994, ApJ, 421, 318
Twarog, B. A., Anthony-Twarog, B., & Tanner, D. 2002, AJ, 123, 2715
Unavane, M., Wyse, R. F. G., & Gilmore, G. 1996, MNRAS, 278, 727
Velázquez, H., & White, D. M. 1999, MNRAS, 304, 254
Venn, K. A., Irwin, M., Shetrone, M. D., et al. 2004, AJ, 128, 1177
Venn, K. A., Irwin, M. J., Pritzl, B. J., & Tout, C. A. 2005, BAAS, 37, 489
Wielen, R. 1977, A&A, 60, 263
Yamagata, T., & Yoshii, Y. 1992, AJ, 103, 117
Yanny, B., Newberg, H. J., Grebel, E. K., et al. 2003, ApJ, 588, 824
Yoachim, P., & Dalcanton, J. J. 2005, ApJ, 624, 701
Yong, D., Carney, B. W., & Teixera de Almeida, M. L. 2005, AJ, 130, 597